

Hunting Nonstandard Neutrino Interactions and Leptoquarks in Dark Matter Experiments

Thomas Schwemmer,^a Volodymyr Takhistov,^{b,c,d,e} Tien-Tien Yu^{a,f}

^a*Department of Physics and Institute for Fundamental Science, University of Oregon
Eugene, Oregon 97403, USA*

^b*International Center for Quantum-field Measurement Systems for Studies of the Universe and Particles (QUP, WPI), High Energy Accelerator Research Organization (KEK),
Oho 1-1, Tsukuba, Ibaraki 305-0801, Japan*

^c*Theory Center, Institute of Particle and Nuclear Studies (IPNS), High Energy Accelerator Research Organization (KEK), Tsukuba 305-0801, Japan*

^d*Kavli Institute for the Physics and Mathematics of the Universe (WPI),
The University of Tokyo Institutes for Advanced Study, The University of Tokyo,
Kashiwa, Chiba 277-8583, Japan*

^e*Graduate University for Advanced Studies (SOKENDAI), 1-1 Oho, Tsukuba, Ibaraki 305-0801, Japan*

^f*Center for Cosmology and Particle Physics, Department of Physics, New York University, New York,
NY 10003, USA*

E-mail: tschwem2@uoregon.edu, vtakhist@post.kek.jp, tientien@uoregon.edu

Abstract: Next generation direct dark matter (DM) detection experiments will have unprecedented capabilities to explore coherent neutrino-nucleus scattering (CE ν NS) complementary to dedicated neutrino experiments. We demonstrate that future DM experiments can effectively probe nonstandard neutrino interactions (NSI) mediated by scalar fields in the scattering of solar and atmospheric neutrinos. We set first limits on S_1 leptoquark models that result in sizable $\mu - d$ and $\tau - d$ sector neutrino NSI CE ν NS contributions using LUX-ZEPLIN (LZ) data. As we show, near future DM experiments reaching $\sim \mathcal{O}(100)$ ton-year exposure, such as argon-based ARGO and xenon-based DARWIN, can probe parameter space of leptoquarks beyond the reach of current and planned collider facilities. We also analyze for the first time prospects for testing NSI in lead-based detectors. We discuss the ability of leptoquarks in the parameter space of interest to also explain the neutrino masses and $(g-2)_\mu$ observations.

Contents

1	Introduction	1
2	Standard Model Neutrino Scattering	3
2.1	Interaction rates and CE ν NS	3
2.2	Neutrino sources	5
3	Nonstandard Neutrino Interactions	8
3.1	Scalar NSI	9
3.2	Vector NSI	10
4	Case Study: Scalar Leptoquarks	10
4.1	The S_1 leptoquark	11
5	Discovery Reach of Dark Matter Detectors	13
5.1	Statistical analysis	13
5.2	Results	14
6	Conclusions	17
	Acknowledgments	17
A	Model extension and neutrino mass	19
B	From leptoquarks to NSI	22
C	Neutrino oscillation effects	23
	Bibliography	32

1 Introduction

Dark matter (DM) constitutes $\sim 85\%$ of all matter in the Universe and understanding its nature is one of the most important goals of science. Significant efforts have been devoted over the past several decades to detect the scattering of particle DM from the Galactic DM halo with target nuclei in underground laboratories. Historically, the focus has been on probing interactions of weakly-interacting massive particles (WIMPs) with masses ~ 100 GeV-TeV, using large ton-scale experiments based on liquid xenon, *e.g.* LUX-ZEPLIN (LZ) [1],

XENONnT [2], and liquid argon, *e.g.* DEAP-3600 [3] and DarkSide-50 [4], detectors. Not only are these detectors very sensitive to the scattering of DM particles with Standard Model (SM) targets, they can also be sensitive to and provide new insights into additional phenomena both within and beyond the SM (BSM).

As direct DM detection experiments continue to improve their sensitivity, they will inevitably encounter an irreducible background stemming from coherent elastic neutrino-nucleus scattering (CE ν NS). Predicted decades ago [5, 6], CE ν NS interactions have been directly observed by COHERENT in 2017 using neutrinos generated by pions that decay at rest [7].¹ Interactions of neutrinos originating from natural sources, such as solar neutrinos from the Sun and atmospheric neutrinos from cosmic ray collisions with the atmosphere, are indistinguishable on an event-by-event basis from DM-induced scattering events depositing energy within detectors (*e.g.* [12–14]). The degeneracy between neutrino and DM scattering results in the so-called “neutrino fog” (formerly known as the “neutrino floor”). Analyses of event statistics and temporal modulation, such as with sidereal day, can help disentangle the degeneracy.

Since the discovery of neutrino oscillations [15], a multitude of experiments have confirmed and further developed the SM picture of neutrino interactions and 3-flavor oscillations [16]. With neutrino physics entering the precision era in a broad, world-wide program including a variety of upcoming major next generation experiments such as DUNE and Hyper-Kamiokande, significant attention is being devoted to probing new neutrino physics. Sizable novel “non-standard” neutrino interactions (NSI) can readily appear (see *e.g.* [17] for review) in broad classes of motivated models, such as those based on SM extensions by an additional $U(1)$ gauge symmetry and new mediators (*e.g.* [18]).

Along with precision tests of SM parameters, observations of CE ν NS, such as data from COHERENT, allow for a unique probe of neutrino NSI and related theoretical models [19–34]. Upcoming next generation DM experiments will have sensitivity to CE ν NS that allows for unique opportunities to test novel neutrino interactions in complementary ways to dedicated neutrino experiments. Studies already initiated exploration of the reach of DM detectors to neutrino NSI [35, 36] mediated by novel scalar, pseudoscalar, vector, and axial-vector particles. Limits on solar neutrino NSI from observations of previous DM experiments have also been explored,² such as from LUX experiment data [38].

In this work, we expand on previous studies and demonstrate the power of DM experiments to probe neutrino NSI. In the case of heavy scalar mediators, the effective interaction becomes a dimension six operator which can either be the familiar NSI modeled after the SM vector-interaction ($\bar{\nu}\gamma^\alpha P_L \nu \bar{q}\gamma_\alpha P_L q$), which is a vector NSI, or a scalar NSI ($\bar{\nu}\nu \bar{q}q$). Our analysis advances the results in the literature in several important ways. While SM interactions of atmospheric neutrinos have been explored in DM experiments [39], we study for the first time

¹Efforts to observe CE ν NS using reactor anti-neutrinos are also being pursued [8–11].

²Neutrino NSI can also be readily probed through electron scattering in DM experiments, which has been recently exploited in attempt to address excess in the XENON1T experiment data [37]. However, in this work we focus solely on CE ν NS interactions.

their potential NSI effects. Furthermore, we explore first constraints on leptoquarks (LQs) and associated theories that can lead to sizable solar and atmospheric neutrino NSI effects in DM experiments, and for the first time use LZ data to set constraints on LQs. We discuss the complementarity of LQ searches in DM experiments and other venues, especially colliders, and connect them with models aiming to address flavor physics observations [40–42], $(g-2)_\mu$, and neutrino mass generation [43–45]. Our analyses are complementary to studies of NSI in DM experiments associated with light mediators, such as Ref. [35, 36, 46–48] or Ref. [49], the latter of which demonstrated that low-threshold (\sim eV) DM detectors are sensitive to light (\sim keV - MeV) mediators where the low energy limit provides an enhancement of the recoil rate.

The paper is organized as follows. In the Sec. 2, we describe the neutrino flux, its flavor composition, and its signal in DM detectors. In Sec. 3 we show the effects of neutrino NSIs and the effective theories that produce such interactions. In Sec. 4 we discuss the details of a UV completion of the effective models as LQs including effects on neutrino masses, $(g-2)_\mu$, and neutrino oscillations. In Sec. 5 we demonstrate the ability of DM detectors to observe the effective models described in Sec. 3, calculate constraints from the LZ experiment, and project the discovery reach of future DM detectors based on xenon, argon, and lead.

2 Standard Model Neutrino Scattering

2.1 Interaction rates and $\text{CE}\nu\text{NS}$

In DM experiments, the recoil rate of neutrinos as a function of the nuclear recoil energy depends on both the physics of the scattering process encapsulated in the cross-section, neutrino energy and flux, as well as the properties of the detector such as target material, size, efficiency, energy threshold, and energy resolution. The general differential recoil rate is given by

$$\frac{dR}{dE'_R} = N_T \int_{E'_R^{\min}} \frac{d\sigma}{dE'_R} \frac{dN_\nu}{dE_\nu} dE_\nu, \quad (2.1)$$

where dN_ν/dE_ν is the neutrino flux, N_T is the number of target nuclei per unit mass (ton) of detector material, $d\sigma/dE'_R$ is process cross-section and for SM $\text{CE}\nu\text{NS}$ it is given by Eq. (2.5). Here, primed energies represent the scattering energy of the interaction while the unprimed energies are those actually measured by the detector. The effects of new physics on the interactions will be explored in Sec. 3. From kinematics, the minimum required neutrino energy to induce a recoil energy E'_R of a nucleus with mass m_N is

$$E_\nu^{\min} = \frac{1}{2} \left(E'_R + \sqrt{E'^2_R + 2E'_R m_N} \right). \quad (2.2)$$

We incorporate the detection efficiency and energy resolution of the detector by integrat-

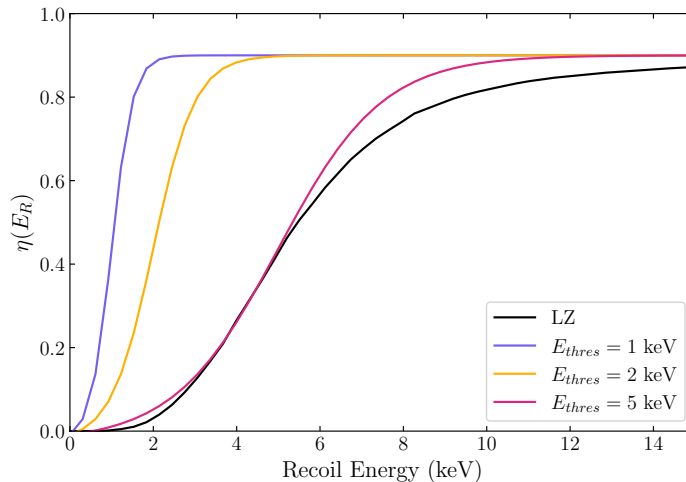


Figure 1: Efficiency models for 1, 2, and 5 keV thresholds compared to LZ experiment data analysis [1]. The sensitivity of DM detectors to NSI is strongly dependent on their energy threshold (*e.g.* [49]). We consider the 2 keV threshold model to be an optimistic efficiency for such near future detectors.

ing over E'_R convoluted with the efficiency and a Gaussian function representing uncertainty

$$\frac{dR}{dE_R} = \int_0^\infty \frac{dR}{dE'_R} \frac{\eta(E'_R)}{\zeta(E'_R)\sqrt{2\pi}} e^{-\frac{(E_R-E'_R)^2}{2\zeta^2(E'_R)}} dE'_R, \quad (2.3)$$

where for $\eta(E'_R)$ we will consider data-driven efficiency function of Eq. (2.4) and $\zeta(E'_R)$ is the energy resolution that we conservatively assume to be $\mathcal{O}(10)\%$ for all energies of interest.³

Focusing on the data analysis from LZ experiment as a characteristic target [1], we model the detection efficiency with a hyperbolic tangent as

$$\eta(E) = \frac{\eta_0}{1 + \zeta} \left(\tanh \xi \left(\frac{E}{E_{\text{th}}} - 1 \right) + \zeta \right), \quad (2.4)$$

where η_0 is the maximum efficiency at high energy, ξ sets the rate of the efficiency rise, E_{th} is the threshold energy, and ζ enforces that the efficiency vanishes at zero recoil energy. We fix $\xi = 2$, which requires $\zeta \approx 0.964$. To approximately match the LZ efficiency, we use $\eta_0 = 0.9$ such that the only remaining parameter is E_{th} , which we vary between 1 and 5 keV. We display the efficiency for a selection of threshold energies in Fig. 1.

Neutrinos that do not possess sufficient energy to discriminate individual nuclear constituents interact with the whole target nucleus via $\text{CE}\nu\text{NS}$ mediated by the weak neutral current [5, 6]. For low momentum transfer $|q|$ satisfying $1/|q| \gg R$, where R is the nuclear radius, the target nucleons interact in phase. $\text{CE}\nu\text{NS}$ is particularly relevant for neutrino

³Our analysis can be readily adapted for other efficiency and resolution functions.

sources with $E_\nu < 50$ MeV, above which other interactions become significant (see *e.g.* [50] for review). Within the SM, CE ν NS interactions are given by

$$\left. \frac{d\sigma_N}{dE_R} \right|_{SM} = \frac{G_F^2}{4\pi} F^2(E_R) Q_v^2 m_N \left(1 - \frac{m_N E_R}{2E_\nu^2} \right), \quad (2.5)$$

where G_F is the Fermi constant, $Q_v = N - Z(1 - 4s_w^2)$ is the weak nuclear charge, N is the number of neutrons, Z is the number of protons, and s_w is the sine of the Weinberg angle. For the atomic mass number $A = N + Z$ and $m_n = 931$ MeV, the nucleus mass is $m_N \approx Am_n$. Here, we employ the Helm nuclear form factor [51, 52]

$$F^2(E_R) = \left[\frac{3j_1(qR_{\text{eff}})}{qR_{\text{eff}}} \right]^2 e^{-(qs)^2}, \quad (2.6)$$

where j_1 denotes spherical Bessel function, $q = \sqrt{2m_N E_R}$ is the transferred 3-momentum, $R_{\text{eff}} = \sqrt{(1.23A^{1/3} - 0.6)^2 + 7\pi^2 r_0^2/3 - 5s^2}$ is the effective nuclear radius, $s = 0.9$ fm is the skin thickness and $r_0 = 0.52$ fm is fit numerically from muon scattering data. With $s_w^2 = 0.232$ [16] CE ν NS interactions scale as $\sim N^2$, signifying sizable enhancement of interaction rates for heavy target materials such xenon, argon, or lead.

2.2 Neutrino sources

A variety of neutrino sources can contribute to irreducible background (*i.e.* giving rise to “neutrino floor/fog”) in direct DM detection experiments, including solar, reactor, geo-, diffusive supernovae background (DSNB) as well as atmospheric neutrinos. For reference, we consider benchmark detector located at SNOLab in Sudbury, Canada that is among likely sites to host next generation DM experiments.⁴

The integrated fluxes for various neutrino components and their uncertainties (rounded to percent level) are listed in Table 1. Contributions from atmospheric, reactor and geo-neutrinos will depend on the location of the experiment. Depending on the experimental energy threshold for nuclear recoil energy E_r , only fluxes resulting in neutrinos with maximum energy $E_\nu^{\text{max}} > E_\nu^{\text{min}}$, where E_ν^{min} is given by Eq. (2.2), will contribute. In Table 1 we display the minimum required energy thresholds in xenon-based and argon-based DM experiments⁵ to detect a particular neutrino source flux. We display the combined solar, DSNB and atmospheric neutrino flux contributions in Fig. 2, along with shaded bands depicting their respective uncertainties.

The keV-level threshold recoils in representative xenon-based experiment require that $E_\nu^{\text{min}} \gtrsim \mathcal{O}(\text{few} \times \text{MeV})$, such that solar (hep and ^8B) background contributions dominate in the region of interest for non-standard neutrino interactions. We include the subdominant atmospheric neutrinos as they are useful in specific UV complete NSI models. A representative

⁴The SNOLab experimental site is located at 46°28′19″ N, 81°11′12″ W with a 6010 meter water equivalent depth.

⁵Considering dominant isotopes, we take $A(Z) = 130$ (54) for xenon and $A(Z) = 40$ (18) for argon.

Neutrino Contribution	Total Flux [$\text{cm}^{-2} \text{ s}^{-1}$]	E_ν^{max} [MeV]	$E_{\text{th}}^{\text{Xe}} (E_{\text{th}}^{\text{Ar}})$ [keV]	Reference (model)
Solar (ν_e , pp)	$5.98(1 \pm 0.01) \times 10^{10}$	0.42	$2.99(9.81) \times 10^{-3}$	[53] (B16-GS98)
Solar (ν_e , pep)	$1.44(1 \pm 0.01) \times 10^8$	1.45	$3.42(11.2) \times 10^{-2}$	[53] (B16-GS98)
Solar (ν_e , hep)	$7.98(1 \pm 0.30) \times 10^3$	18.77	5.74(18.9)	[53] (B16-GS98)
Solar (ν_e , ${}^7\text{Be}$)	$4.93(1 \pm 0.06) \times 10^9$	0.39	$1.20(3.96) \times 10^{-2}$	[53] (B16-GS98)
Solar (ν_e , ${}^8\text{B}$)	$5.46(1 \pm 0.12) \times 10^6$	16.80	4.58(15.1)	[53] (B16-GS98)
Solar (ν_e , ${}^{13}\text{N}$)	$2.78(1 \pm 0.15) \times 10^8$	1.20	$2.33(7.65) \times 10^{-2}$	[53] (B16-GS98)
Solar (ν_e , ${}^{15}\text{O}$)	$2.05(1 \pm 0.17) \times 10^8$	1.73	0.0486(0.160)	[53] (B16-GS98)
Solar (ν_e , ${}^{17}\text{F}$)	$5.29(1 \pm 0.20) \times 10^6$	1.74	0.0492(0.161)	[53] (B16-GS98)
Atm. (ν_e) ¹	$1.27(1 \pm 0.50) \times 10^1$	944	$1.47(5.00) \times 10^4$	[54] (FLUKA)
Atm. ($\bar{\nu}_e$)	$1.17(1 \pm 0.50) \times 10^1$	944	$1.47(5.00) \times 10^4$	[54] (FLUKA)
Atm. (ν_μ)	$2.46(1 \pm 0.50) \times 10^1$	944	$1.47(5.00) \times 10^4$	[54] (FLUKA)
Atm. ($\bar{\nu}_\mu$)	$2.45(1 \pm 0.50) \times 10^1$	944	$1.47(5.00) \times 10^4$	[54] (FLUKA)
DSNB (ν_e) ³	$4.55(1 \pm 0.50) \times 10^1$	36.90	22.1(72.7)	[55] (th. avrg.) ²
DSNB ($\bar{\nu}_e$)	$2.73(1 \pm 0.50) \times 10^1$	57.01	52.8(174)	[55] (th. avrg.) ²
DSNB (ν_x) ⁴	$1.75(1 \pm 0.50) \times 10^1$	81.91	109(359)	[55] (th. avrg.) ²
Reactor ($\bar{\nu}_e$, ${}^{235}\text{U}$) ⁵	$1.88(1 \pm 0.08) \times 10^5$	10.00	1.62(5.33)	[14](combined) ⁶
Geo. ($\bar{\nu}_e$, ${}^{40}\text{K}$)	$2.19(1 \pm 0.17) \times 10^7$	1.32	$2.83(9.29) \times 10^{-2}$	[56] (global) ⁶
Geo. ($\bar{\nu}_e$, ${}^{238}\text{U}$)	$4.90(1 \pm 0.20) \times 10^6$	3.99	0.259(0.849)	[56] (global) ⁶
Geo. ($\bar{\nu}_e$, ${}^{232}\text{Th}$)	$4.55(1 \pm 0.26) \times 10^6$	2.26	$8.29(27.2) \times 10^{-2}$	[56] (global) ⁷

¹ The cut-off of Fluka analysis.

² Average of several theoretical models.

³ Fermi-Dirac spectrum with neutrino temperature of $T_\nu = 3, 5, 8$ MeV for $\nu_e, \bar{\nu}_e, \nu_x$, respectively.

⁴ ν_x is the total contribution from all other neutrinos and antineutrinos.

⁵ Only the most dominant element is considered.

⁶ Combined result from multiple nearby reactors.

⁷ Global Earth model, incorporates several theoretical models.

Table 1: Neutrino flux components that contribute to the coherent neutrino scattering background in direct detection experiments at the SNOLab location. Contributions from solar, atmospheric, diffuse supernovae, reactor as well as geo-neutrinos are shown.

figure for scalar-mediated non-standard neutrino interactions are displayed in Fig. 3, further discussed below in Sec. 3.

Solar neutrinos: The majority of neutrinos reaching the Earth’s surface are produced in nuclear fusion processes in the Sun (for review see *e.g.* [57, 58]). The flux and energy spectrum of solar neutrinos depends on the specific nuclear reaction chain step that produces them.

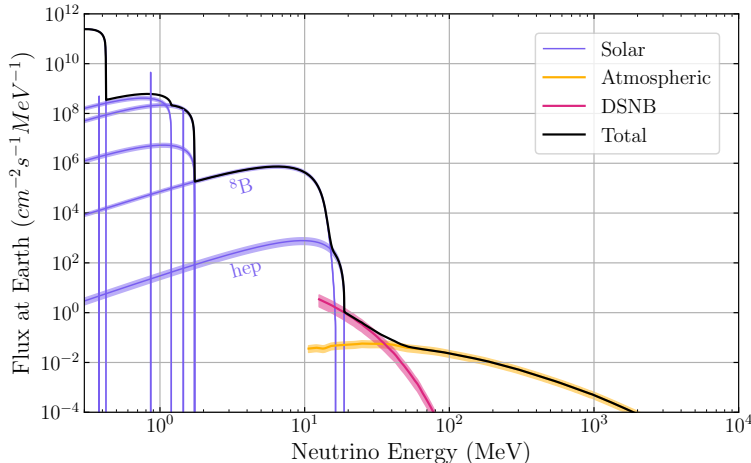


Figure 2: Neutrino flux contributions including solar, atmospheric, and DSNB components and their respective uncertainties on the surface of the Earth considering SNOLab detector location. See text and Table 1 for additional details.

The vast majority of Sun’s energy, nearly 99%, originates from proton-proton (pp) chain reactions, producing pp, hep, pep, ${}^7\text{Be}$, ${}^8\text{B}$ neutrinos. The remaining $\sim 1\%$ of Sun’s energy originates from Carbon-Nitrogen-Oxygen (CNO) cycle, producing ${}^{13}\text{N}$, ${}^{15}\text{O}$, ${}^{17}\text{F}$ neutrinos.

For $E_\nu \lesssim 20$ MeV energies, solar neutrinos dominate background for direct DM detection experiments. In this work we employ solar neutrino fluxes of high metallicity solar model B16-GS98 [53], favored by recent Borexino neutrino observation data analysis [59]. The dominant neutrino background contribution for a range of parameters stems from ${}^8\text{B}$ neutrinos.

DSNB: For neutrino energies around $20 \text{ MeV} \lesssim E_\nu \lesssim 50 \text{ MeV}$ DSNB significantly contributes to neutrino background fluxes [60]. Around 99% of the gravitational binding energy is released in the form of neutrinos in core-collapsing supernova, resulting in $\sim 10^{58}$ neutrinos emitted yielding about $\sim 10^{53}$ ergs in energy. The DSNB denotes combined contributions of neutrinos originating from all the historic core-collapse supernovae events. The DSNB flux is formed from convolution of the redshift-dependent core-collapse supernovae rate, which is found from initial stellar mass function and star formation rate, as well as emitted core-collapse neutrino spectrum. Approximating the emitted neutrino spectra as thermal, we consider DSNB neutrinos characterized by temperature T_ν averaged for each species over theoretical models in Ref. [55]. Significant efforts are underway by neutrino experiments, especially Super-Kamiokande [61], to detect the DSNB in the near future.

Atmospheric neutrinos: For $E_\nu \gtrsim 50$ MeV, neutrino contributions become dominated by neutrinos produced from cosmic ray collisions with nuclei in the atmosphere (see *e.g.* [62] for review). Such interactions produce copious amounts of π^\pm and K^\pm mesons that predominantly decay to $\mu^+ + \nu_\mu$ and $\mu^- + \bar{\nu}_\mu$, followed by muon decay to electrons and pairs of neutrinos resulting in a ν_μ and $\bar{\nu}_\mu$ flux twice that of ν_e and $\bar{\nu}_e$. The atmospheric neutrino flux carries an $\mathcal{O}(30\%)$ theoretical uncertainty, which we take to be 50% conservatively, due

to the uncertainty in the cosmic ray flux and its propagation in the magnetic fields of the Earth and solar system. In addition to this uncertainty, the flux varies significantly though predictably with the position of the detector and the phase in the solar cycle [63].

Neutrino Oscillations: As shown in Table 1, solar neutrinos are produced as electron neutrinos. Since these neutrinos have a much longer baseline than those in reactor experiments, neutrino oscillations result in a significant fraction of neutrinos reaching the detector with μ - or τ -components, allowing experiments to constrain interactions of second and third generation neutrinos.

Neutrino oscillations in matter are further complicated by the Mikheyev–Smirnov–Wolfenstein (MSW) effects [64]. The matter potential $V_{\text{MSW}} = \sqrt{2}G_F n_e \text{diag}(1, 0, 0)$, where n_e is the electron number density, modifies the neutrino oscillation Hamiltonian as

$$\mathcal{H}_{\text{matter}} = E_\nu + \frac{MM^\dagger}{2E_\nu} + V_{\text{MSW}} . \quad (2.7)$$

Vector NSI contribute to the matter potential analogously to MSW effects [65]. Scalar NSI contribute a new mass-like term, which has inverse neutrino energy dependence and hence suppressed at higher neutrino energies [66]. We consider these effects and include in oscillation analysis as discussed in Appendix C. Throughout, we assume normal neutrino mass ordering.

3 Nonstandard Neutrino Interactions

There are several formalisms to incorporate general interactions of neutrinos (see *e.g.* [67]). One system of simplified models which has gained popularity generates NSI by introducing new mediators which couple to neutrinos and normal fermions as outlined in Ref. [36], also employed in *e.g.* Ref. [49, 68]. categorizes interactions by the Lorentz structure of the mediator such that interactions are defined as scalar, pseudoscalar, vector, axial vector, and tensor (SPVAT). Specifically, we focus on scalar mediators with masses above ~ 1 TeV, which allows us to map our general interactions to effective four-Fermi interactions at low energies which are recognizable in the conventional language of NSI [67].

In this work, we will consider either flavor independent couplings of a generalized scalar interaction, or what is often called a “minimal coupling” scenario, in which all couplings are zero except the one of interest that couples a particular flavor of neutrino with a specific quark. The latter is typically more useful in mapping to UV complete models, and example of which we show in Sec. 4. For this case although the form of the cross-section is flavor-independent, the fluxes vary as discussed in Sec. 2. This means that for a comprehensive treatment of a scalar coupled to multiple flavors one would need to calculate the scattering of each flavor independently and combine the signals. Additionally, we are primarily interested in couplings to first generation quarks as this is where DM experiments are sensitive as we discuss in Sec. 5. In Sec. 3.1 we provide the expressions for scalar NSI and in Sec. 3.2, we do the same for vector NSI.

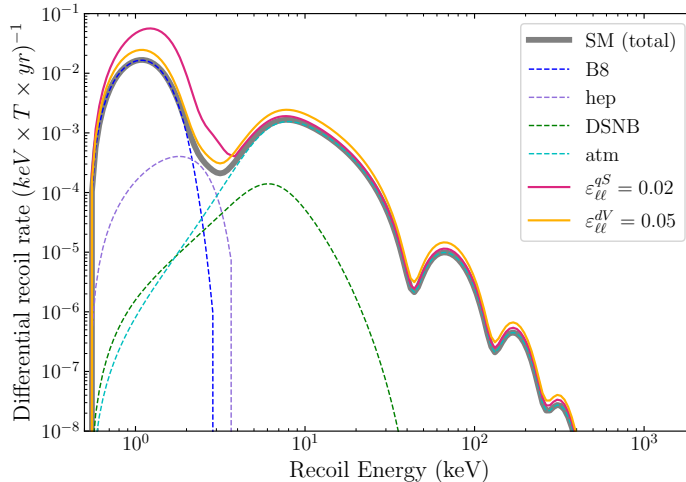


Figure 3: Recoil rates in a xenon detector with a 5 keV threshold for SM interactions of neutrinos (dashed lines), with B8, hep, DSNB, and atmospheric neutrino sources, and the total (thick grey line) as well as the total including a scalar NSI (magenta) for $\varepsilon_{\ell\ell}^{qS} = 0.02$ for all q and ℓ .

3.1 Scalar NSI

The effective Lagrangian for scalar NSI with Dirac neutrinos is given by [66]

$$\mathcal{L}_{sNSI} \supset G_F \sum_{q,\alpha,\beta} \varepsilon_{\alpha\beta}^{qS} \bar{\nu}_\alpha \nu_\beta \bar{q} q, \quad (3.1)$$

where the interaction is a dimension six operator suppressed by two powers of a large mass scale. The indices q run over the quark flavors, while α, β run over the lepton flavors. In this work, we will consider flavor-conserving interactions, $\alpha = \beta = \ell$. Scalar NSI cannot be converted to conventional vector-like NSI by Fierz transformations since they arise from a neutral scalar mediator [69]. On the other hand, as we will discuss in Sec. 4, a charged (colored) scalar produces a conventional vector NSI after Fierz transformations.

The scalar NSI effective vertex gives rise to an additional contribution to the $CE\nu$ NS cross-section:

$$\left. \frac{d\sigma}{dE_R} \right|_S = \frac{F^2(E_R) G_F^2 \varepsilon_{q\ell}^2 q_S^2 E_R m_N^2}{4\pi E_\nu^2}, \quad (3.2)$$

where E_R is the energy of the recoiling quark, m_N is the nuclear mass, and q_S is the effective scalar charge of the nucleus. In the flavor/generation independent case, we have $q_S \approx 14A + 1.1Z$ [36]. A sample of the differential recoil rate, both from the SM and NSI is shown in Fig. 3.

3.2 Vector NSI

The effective Lagrangian for a vector NSI is

$$\mathcal{L}_{NSI} = -2\sqrt{2}G_F \sum_{q,\alpha,\beta} \varepsilon_{\alpha\beta}^{qP} (\bar{\nu}_\alpha \gamma^\mu P_L \nu_\beta) (\bar{q} \gamma_\mu P q) , \quad (3.3)$$

where $P = P_L, P_R$ are the projection operators. As with the neutral scalar, we assume flavor-conserving NSI, that is, $\alpha = \beta = \ell$. Similarly, we assume the interaction conserves quark flavor. Vector NSIs can be parameterized in terms of vector ($\varepsilon_{\ell\ell}^{qV} = \varepsilon_{\ell\ell}^{qL} + \varepsilon_{\ell\ell}^{qR}$) and axial ($\varepsilon_{\ell\ell}^{qA} = \varepsilon_{\ell\ell}^{qL} - \varepsilon_{\ell\ell}^{qR}$) components.

In the case of CE ν NS, the vector component of the interaction gets enhanced by the size of the nucleus while the axial component is proportional to the nuclear spin. This results in a $1/A$ suppression of the axial component relative to the vector part. As in [19], we drop the axial component and consider only the vector component of the interaction. The scattering cross-section for vector NSI is given by

$$\left. \frac{d\sigma}{dE_R} \right|_{NSI} = \frac{F^2(E_R) G_F^2 Q_{NSI}^2 m_N}{2\pi E_\nu^2} (2E_\nu^2 - m_N E_R) . \quad (3.4)$$

In Eq. (3.4), Q_{NSI} is the change in the effective nuclear coupling induced by the NSI and given by

$$Q_{NSI}^2 = \left[Q_{SM} + (2\varepsilon_{\ell\ell}^{uV} + \varepsilon_{\ell\ell}^{dV}) Z + (\varepsilon_{\ell\ell}^{uV} + 2\varepsilon_{\ell\ell}^{dV}) N \right]^2 - Q_{SM}^2 \quad (3.5)$$

for a nucleus with Z protons and N neutrons. θ_W is the Weinberg angle and $Q_{SM} = [(1/2 - 2\sin^2(\theta_W)) Z - N/2]$ is the SM contribution to the neutrino-nuclear coupling. In general, since the $\varepsilon_{\ell\ell}^{qV}$ parameters can be positive or negative, there exists parameter space for a given detector material where the up and down couplings cancel and the NSI does not change the scattering rate.

In what follows, we will study two cases which we call “flavor universal” and “minimal” NSI, where “flavor universal” means $\varepsilon_{ee} = \varepsilon_{\mu\mu} = \varepsilon_{\tau\tau}$. In the scalar NSI case, this extends to the quark sector as well, that is $\varepsilon_{\ell\ell}^{uS} = \varepsilon_{\ell\ell}^{dS}$. In the vector NSI case, we note it is impossible for a singlet scalar to have both $\varepsilon_{\ell\ell}^{dV}$ and $\varepsilon_{\ell\ell}^{uV}$ while conserving electric charge, so in the case of vector NSI, “flavor universal” refers only to lepton flavors. “Minimal” NSI means $\varepsilon_{\ell\ell}^{qV} \neq 0$ for only one flavor of ℓ and q .

4 Case Study: Scalar Leptoquarks

We will demonstrate how models of leptoquarks (LQs), which interact with baryons and leptons, provide an example application of our formalism. LQs are theoretically well-motivated and naturally arise in the context of Grand Unification theories such as $SU(5)$ [70] and $SU(10)$ [71, 72], as well as the Pati-Salam models that unify quark and leptons [73]. Further, they can manifest in R -parity violating models of supersymmetry [74, 75].

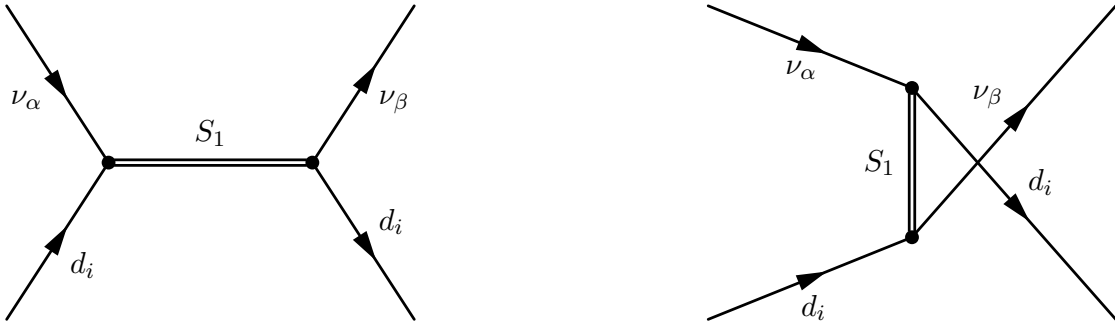


Figure 4: Neutrino-quark scattering mediated by the S_1 scalar leptoquark.

LQs have been recently connected to possible observational anomalies in semi-leptonic B decays [40, 41, 76, 77]. In addition, scalar LQs have been posed as solutions to the neutrino mass problem [43, 45] (see Appendix A for an example). If the LQ couples to muons, it provides a contribution to the anomalous magnetic moment at one loop order and may be part of the explanation for the anomalous magnetic moment of the muon $(g - 2)_\mu$ [42, 44, 78, 79].

Here, we consider LQs in the large coupling regime, which are of interest for observations and provide a heavy scalar that couples to both quarks and neutrinos [80, 81]. To map the LQ models to the NSIs discussed above, we note that because the mediator carries lepton and quark quantum numbers, the interactions proceed via s and u -channel diagrams rather than the t -channel of uncharged scalar interactions (see Fig. 4). Once the massive fields are integrated out, a Fierz transformation leads to an effective four-fermion vertex identical to the vector NSI Sec. 3.2. We derive the vector NSI parameters in Sec. B.

4.1 The S_1 leptoquark

We will focus on scalar LQs as the simplest realization of neutrino NSIs. As a concrete realization, we consider the $S_1 = (\bar{3}, 1, 1/3)$ leptoquark, where parenthesis represent transformation under SM $(SU(3), SU(2), U(1))$ symmetries. The additional relevant Lagrangian terms due to S_1 are [82–84]:

$$\mathcal{L}_{S_1} \supset -m_{S_1}^2 |S_1|^2 + (\lambda_L^{i\ell} S_1 \bar{Q}_i^c \epsilon L_\ell + \lambda_R^{i\ell} S_1^* \bar{u}_R^i \bar{\ell}_R + h.c.), \quad (4.1)$$

where $Q_i = (u_L, d_L)_i$ and $L_\ell = (\nu_{\ell L}, \ell_L)$ are the left-handed quark and lepton doublets respectively, ℓ is the lepton flavor, ϵ is the Levi-Civita tensor, and i is the quark generation index. From expansion of the $SU(2)$ -doublets in Eq. (4.1), we note that the same Yukawa interaction that couples charged leptons to up-type quarks will couple neutrinos to down-type quarks. Thus, by constraining neutrino scattering, we also place constraints on the charged lepton S_1 couplings. Throughout, we do not consider possible effects of diquark terms, which could lead to nucleon decay. Such terms can be readily restricted by additional symmetries, however detailed model implementation is beyond the scope of the present work.

As stressed in Refs. [80, 85], without a model-independent reason dictating a flavor pattern of LQ couplings all nine quark-lepton generation pairings are possible. Strong constraints exist on the first generation couplings, λ^{qe} , particularly from atomic parity violating experiments [80, 83, 86, 87]. Here, we shall focus on LQ couplings to the μ and τ flavored leptons. For simplicity, we will also assume the LQ couples only to one-generation (sometimes called the “minimal leptoquark” [80]), either μ or τ leptons.⁶

The interactions of S_1 LQ can lead to distinct phenomenological consequences. Through the coupling to μ -sector the S_1 LQ can directly contribute to the magnetic moment of the muon. For $m_{S_1} \gg m_t$ the resulting contribution to $a_\mu = (g - 2)_\mu/2$ is [89]

$$a_\mu^{S_1} = \sum_i \frac{m_\mu m_{u_i}}{4\pi^2 m_{S_1}^2} \left(\ln m_{S_1}^2/m_{u_i}^2 - 7/4 \right) \Re(\lambda_R^{*i2} \lambda_L^{i2}) - \frac{m_\mu^2}{32\pi^2 m_{S_1}^2} \left(\sum_i |\lambda_R^{i2}|^2 + \sum_i |\lambda_L^{i2}|^2 \right), \quad (4.2)$$

which is dominated by the term proportional to the up-type quark masses. In a LQ model where the charm and top quarks have the same coupling as the up-quark, we can estimate a favored region in the LQ mass vs. up-type Yukawa plane that alleviates the $(g - 2)_\mu$ anomaly. This region is indicated with a grey band in Fig. 6. In the case that the coupling to charm and top quarks vanishes or $\lambda_R \ll \lambda_L$, the second term dominates and exacerbates the anomaly.

Since we are interested in coupling to protons and neutrons, we restrict ourselves to couplings to first generation of SM quarks. We are considering neutrino-nuclear scattering in or near the elastic regime, so the parton distribution functions (PDFs) are dominated by the first generation quarks.⁷ Thus, we consider scalar S_1 LQ with couplings $\lambda^{d\ell}$, where $\ell = \mu, \tau$.

With these assumptions and for an $\mathcal{O}(\text{TeV})$ LQ, we can integrate out the LQ field, perform a Fierz transformation, and map the resulting dimension six operator back to the NSI parameters in eq. (3.3) as

$$\varepsilon_{\ell\ell, S_1}^{dV} = \frac{-|\lambda_L^{d\ell}|^2}{4\sqrt{2}G_F m_{S_1}^2}. \quad (4.3)$$

We provide details on this calculation in Appendix B. Note the interactions only involve down-type quarks, which is accounted for by a change in the effective charge Q_{S_1} .

$$Q_{S_1} = Z \left(\frac{1}{2} - 2 \sin^2(\theta_W) + \varepsilon_{\ell\ell, S_1}^{dV} \right) + N \left(-\frac{1}{2} + 2\varepsilon_{\ell\ell, S_1}^{dV} \right), \quad (4.4)$$

Lastly, we are considering the “minimal LQ” model in which the S_1 couples to a single flavor of neutrinos, such that the neutrino-nuclear scattering signal only involves a single neutrino-flavor. Note that this is contrast to SM CE ν NS, which involve all flavors.

⁶The flavor-changing constraints in this case are much weaker and couplings to both μ and τ may be simultaneously allowed as long as one coupling is marginally smaller than the other [88].

⁷This neglects the “sea quarks” which provide trace amounts of anti-quarks of the first generation as well as (even fewer) strange quarks and anti-quarks. In principle, these sea quarks provide an effective charge allowing detection of NSIs coupled to strange quarks or, as in the case of the \tilde{R}_2 LQ (defined in Appendix A), NSIs which only couple neutrinos to anti-quarks (or quarks to anti-neutrinos), though the PDF suppression is such that neutrino scattering is not a competitive means to set bounds.

5 Discovery Reach of Dark Matter Detectors

We are interested in calculating the potential of a DM direct detection experiment to uncover signals of neutrino NSIs, with the SM CE ν NS as our effective background. In the following analysis, we will present our results in terms of the general NSI parameters $\varepsilon_{\ell\ell}^{qS}$ and in terms of the LQ model parameters, $\lambda_{S_1}^{d\ell}, m_{S_1}$, from the previous section. For generality, we will consider that we are dominated by statistics and do not focus on making predictions in the context of more detector-specific systematic backgrounds, such as radioactive decay in or near the detector, or any other instrumental noise. Neutrino oscillation effects are present for both scalar and vector NSIs, though as we discuss in Appendix C, these effects are minimal for the NSI parameters we consider and are not included in the following analysis. We also do not consider the presence of a DM signal in this analysis, although Ref. [38] studied the effect of NSIs on the neutrino fog.

5.1 Statistical analysis

Since we have reduced the NSI cross-section to one free parameter, $\varepsilon_{\ell\ell}^{qS}$, we use a likelihood ratio method to project the significance of simulated data. This follows the method used for the magnetic moment calculation in Ref. [49], which was also dependent on only one parameter. We take as our likelihood function

$$\mathcal{L}(\varepsilon, \vec{\phi}) = \frac{e^{-\sum_{j=1}^{n_\nu} (\eta_{\varepsilon,j} + \eta_{SM,j})}}{N!} \times \prod_{j=1}^{n_\nu} \mathcal{L}(\phi_j) \times \prod_{i=1}^N \left(\sum_{j=1}^{n_\nu} (\eta_{\varepsilon,j} f_{\varepsilon,j}(E_i) + \eta_j f_{SM,j}(E_i)) \right), \quad (5.1)$$

where we have dropped the labels on $\varepsilon = \varepsilon_{\ell\ell}^{qS}$ for simplicity, n_ν label the neutrino fluxes and N labels the energy bins. Here, $\vec{\phi}$ are nuisance parameters normalizing the neutrino flux channels. They are allowed to fluctuate weighted by Gaussian distribution,

$$\mathcal{L}(\phi_j) = \frac{1}{\sigma_j \sqrt{2\pi}} e^{-\frac{1}{2} \left(\frac{\phi_j - \phi_{0,j}}{\phi_j} \right)^2}, \quad (5.2)$$

where the width of their uncertainties, σ_j is given in Table 1. The functions $f_{\varepsilon,j}(E_i)$ and $f_{SM,j}(E_i)$ are the distribution functions (*i.e.* the normalized rates) for the number of events in the i -th energy bin from the j -th neutrino flux from NSI (ε) or SM scattering. $\eta_{\varepsilon,j}$ and $\eta_{SM,j}$ are the number of events predicted from the NSI or SM in each channel (j) based on the nuisance parameters. The latter depends only on the normalization of the neutrino flux components while the former depends on both the flux normalization and the NSI parameter (ε). The product over i runs over the number of events in the simulated data.

For a particular data set, we maximize the likelihood with $\varepsilon = 0$ as our null hypothesis and $|\varepsilon| > 0$ for NSI signals. If the null likelihood is greater than the signal likelihood, we assign the significance $\sigma = 0$. If $\mathcal{L}(\varepsilon \neq 0)/\mathcal{L}(\varepsilon = 0) \equiv \lambda > 1$, we have a test statistic $t = 2 \log(\lambda)$ and significance $\sigma = \sqrt{t}$. This analysis is run on 600 of sets of pseudo-data generated by Poisson

fluctuating the expected rates for a given $\varepsilon_{\ell\ell}^{qS}$ and exposure. The average of these data sets is then used for the projections in Sec. 5.2.

5.2 Results

In this section, we present the results of the likelihood procedure described in the previous section. We show the 3σ and 5σ contours for ε in the exposure- ε plane in Fig. 5, for a flavor universal scalar ($\varepsilon_{\ell\ell}^{qS}$, upper left) and a minimal scalar ($\varepsilon_{\ell\ell}^{dS}$, upper right) while the equivalent contours for vector NSI are shown in the lower panels. We find that the discovery regions of the experiments we consider are within the range of values allowed by IceCube ($-0.041 < \varepsilon_{\ell\ell}^{qV} < 0.042$) [90] and Super-Kamiokande ($-0.049 < \varepsilon_{\ell\ell}^{qV} < 0.049$) [91]. For the flavor universal scalar, we show the effects of varying the detector energy threshold. The yellow curves show the reach using the efficiency from the LZ experiment [1]. Improving the detector efficiency can lead to a significantly stronger reach, and we see that lowering the detector threshold from $E_{\text{th}} = 2$ keV to 1 keV improves the reach on ε by about a factor of few. Since $P_{e\rightarrow\tau} > P_{e\rightarrow\mu}$ when averaged over the solar neutrino spectrum, there will be ~ 3 ν_τ for every 2 ν_μ , thus we expect τ constraints to be stronger by a factor $\sim \sqrt{3/2}$. This is confirmed by the results in Fig. 5 where we also show the results of an analysis of only atmospheric neutrinos which are useful to constrain interactions with anti-neutrinos such as the \tilde{R}_2 LQ (see Appendix A). We further display how the results will improve as atmospheric neutrino flux uncertainty is further reduced, as far down as optimistic $\mathcal{O}(1\%)$ -level.

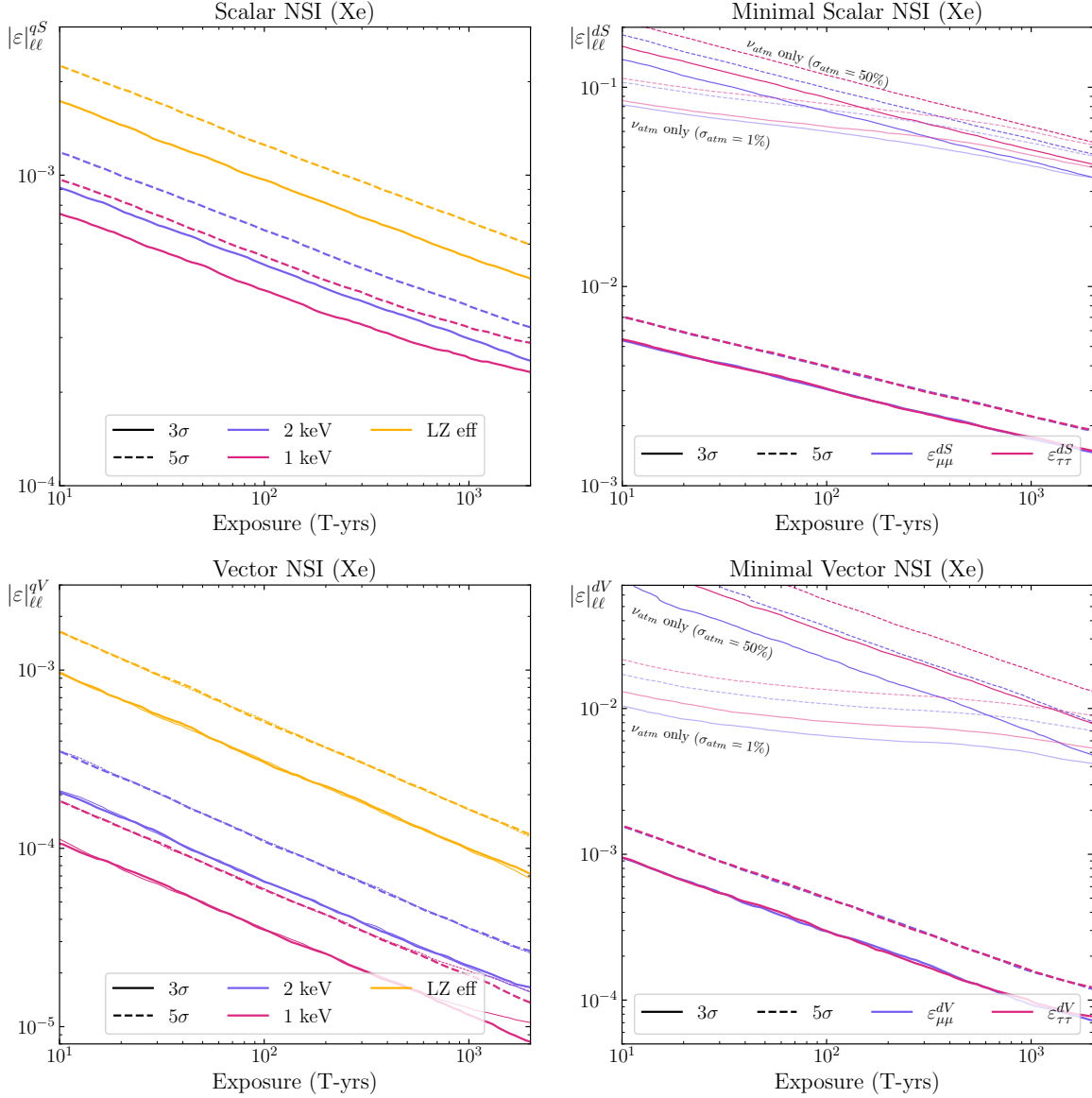


Figure 5: Left: 3σ (solid) and 5σ (dashed) discovery reach of a xenon detector for an NSI with universal couplings ($\varepsilon_{ee}^{dV} = \varepsilon_{\mu\mu}^{dV} = \varepsilon_{\tau\tau}^{dV}$) as a function of detector exposure, for a 1 keV (magenta) and 2 keV (purple) detector threshold as defined in Sec. 2.1. Also shown is the reach using the LZ efficiency and threshold (yellow). As expected, a lower threshold improves the discovery reach. **Right:** discovery reach of a xenon detector to NSIs coupling only the d quark to either ν_μ or ν_τ , assuming a 2 keV threshold. Thin lines indicate the sensitivity based only on atmospheric neutrinos. Fainter lines show the improvement to be gained from more precise measurement of the atmospheric neutrino flux with reduced uncertainties. Upper panels show results for scalar NSI while lower panels are vector NSI results. In the vector NSI panels, we present results for both $\varepsilon < 0$ ($\varepsilon > 0$) with the thick (thin) lines, and show that they are similar. The lower right panel maps to the S_1 LQ parameters in Fig. 6.

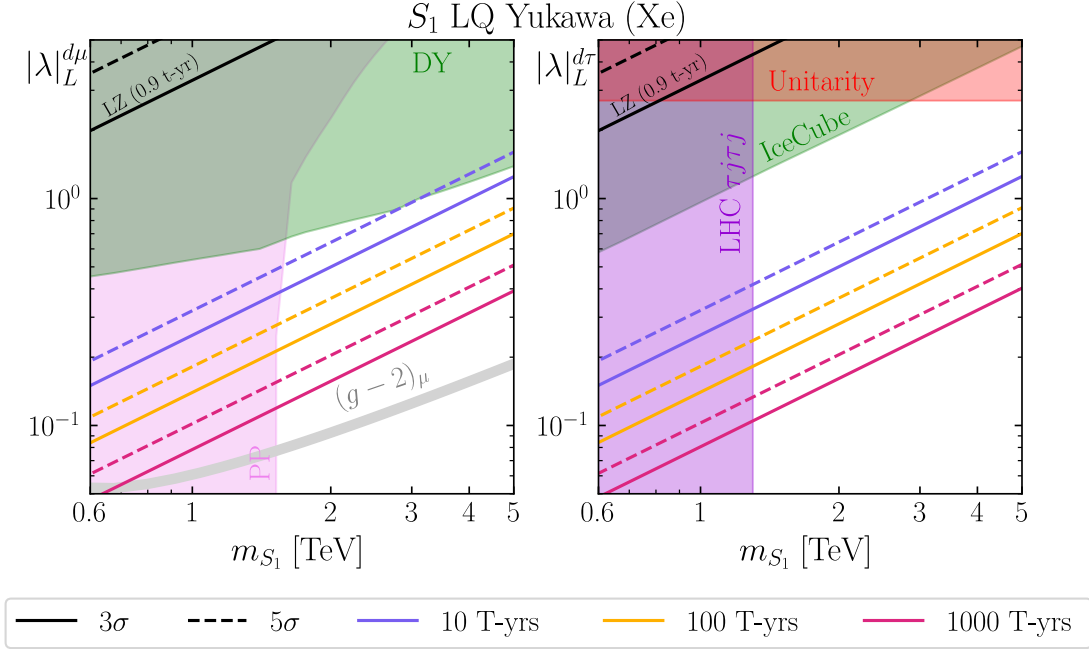


Figure 6: Projected constraints on the $\mu - d$ (left) and $\tau - d$ (right) Yukawas for a selection of exposures, mapped from sensitivity to a $\varepsilon_{\ell\ell}^{dV}$ minimal NSI in a xenon DM detector with a 2 keV threshold. Dashed (solid) lines represent 5 σ and 3 σ sensitivity reach. We set the first limits on LQs from preliminary LZ data with 0.9 ton-year exposure [92]. In the $d - \mu$ figure (left), the thick grey line indicates the preferred values to alleviate the $(g - 2)_\mu$ anomaly for quark generation and chirality independent couplings. Pair production (PP) and Drell-Yan (DY) bounds on the muon coupling are from 36 fb $^{-1}$ data from the LHC [93, 94]. In the $d - \tau$ figure (right), we show the LHC bounds on the tau coupling [95] which constrain $m_{LQ} > 1.3$ TeV. IceCube results are from resonance searches in atmospheric neutrino data [96]. At the highest masses, the LQ Yukawa coupling is only constrained by perturbative unitarity [97].

We also present our results in terms of the scalar LQ S_1 parameters, $\lambda^{d\ell}$ and m_{S_1} , in Fig. 6 for a few select detector exposures. Our work, for the first time, shows the constraints from the LZ experiment in black. In addition, we show constraints from the LHC searches looking for LQ pair production (PP) and Drell-Yan (DY) production using 36 fb $^{-1}$ of data [93, 94]. As seen in Fig. 6, the DM direct detection constraints are competitive with the LHC constraints for the $\lambda^{d\mu}$, but do not access the parameter region relevant for $(g - 2)_\mu$ shown in gray. The DM direct detection constraints are significantly stronger than the LHC constraints for $\lambda^{d\tau}$, where the mass and short lifetime of the charged τ weaken the LHC constraints [80], and the IceCube constraints coming from atmospheric neutrinos [90]. For both scenarios, there are constraints from perturbative unitarity [97], which provide the strongest constraints on $\lambda^{d\tau}$ for $m_{S_1} \gtrsim 3$ TeV.

In addition to xenon, other DM experiments can also have enhanced sensitivity to CE ν NS and related new physics. In general, the effective charge of the nucleus grows as the square

of its mass, so for a given detector target mass, larger nuclei are expected to result in more events even though there are fewer target nuclei. This competes with the kinematic effects whereby higher intensity but lower energy neutrinos are often pushed below threshold in detectors with heavy nuclei.

In figures 7 and 8 we display the 3σ and 5σ discovery reach contours for the NSI parameter ε in the exposure- ε plane for argon and lead-based detectors. For estimating the sensitivity to scalar NSIs, while the details depend on the specific experimental configuration, we assume for simplicity the same threshold and efficiency parameters as for xenon-based detector. Note that argon does not see much improvement as the threshold falls below 5 keV (the differences seen above are statistical noise). Argon has a relatively light nucleus and the peak induced by boron-8 is at higher energy, so lowering the threshold does not increase the number events as efficiently until the oxygen-16 neutrinos have an effect (below ~ 0.5 keV). For the heavier lead nucleus, recoils induced by boron-8 neutrinos are partially cut by the threshold, so improving the threshold makes a much larger number of recoils accessible. The lower panels of figures 7 and 8 show the sensitivity to minimal couplings assuming the 2 keV threshold and efficiency.

In Fig. 9, we translate our results into sensitivity projections for scalar LQ S_1 parameters, $\lambda_L^{q\ell}$ and m_{S_1} , as before. We find that a detector constructed from either material, argon or lead, and reaching multi-ton-year exposure can be sensitive and improve existing bounds on the S_1 LQ couplings.

6 Conclusions

Direct DM detection experiments constitute a central pillar in the search for DM and will continue to increase their exposures and lower thresholds and backgrounds. As we demonstrate, this will allow such experiments to constrain or reveal new physics in the space of neutrino interactions, complementary to conventional neutrino telescopes. We set new limits on LQs associated with scalar neutrino NSI using latest data of direct DM detection experiments, in particular LZ. We find that near-future DM detectors can probe parameter space of LQs that is out of reach of the LHC. We discuss how upcoming measurements improving uncertainties for atmospheric neutrino could probe LQ and NSI parameter space. The studied LQs are of particular interest for interpreting the observations of $(g-2)_\mu$ and explaining neutrino masses. Our analysis can be extended to variety of other models and similar methodology could also be applied to vector-like LQs, which may be associated with measurements and anomalies in flavor physics. Such a realization of massive scalar mediated NSIs provides a new benchmark for testing new physics beyond the SM at planned near-future experiments.

Acknowledgments

We thank Pouya Asadi, Kaladi Babu, Bhupal Dev, Bhaskar Dutta, Motoi Endo, Danny Marfatia for helpful discussions. T.S. and T.-T.Y. were supported in part by NSF CAREER grant PHY-1944826. T.-T.Y. also thanks the CCPP at NYU for hospitality and support.

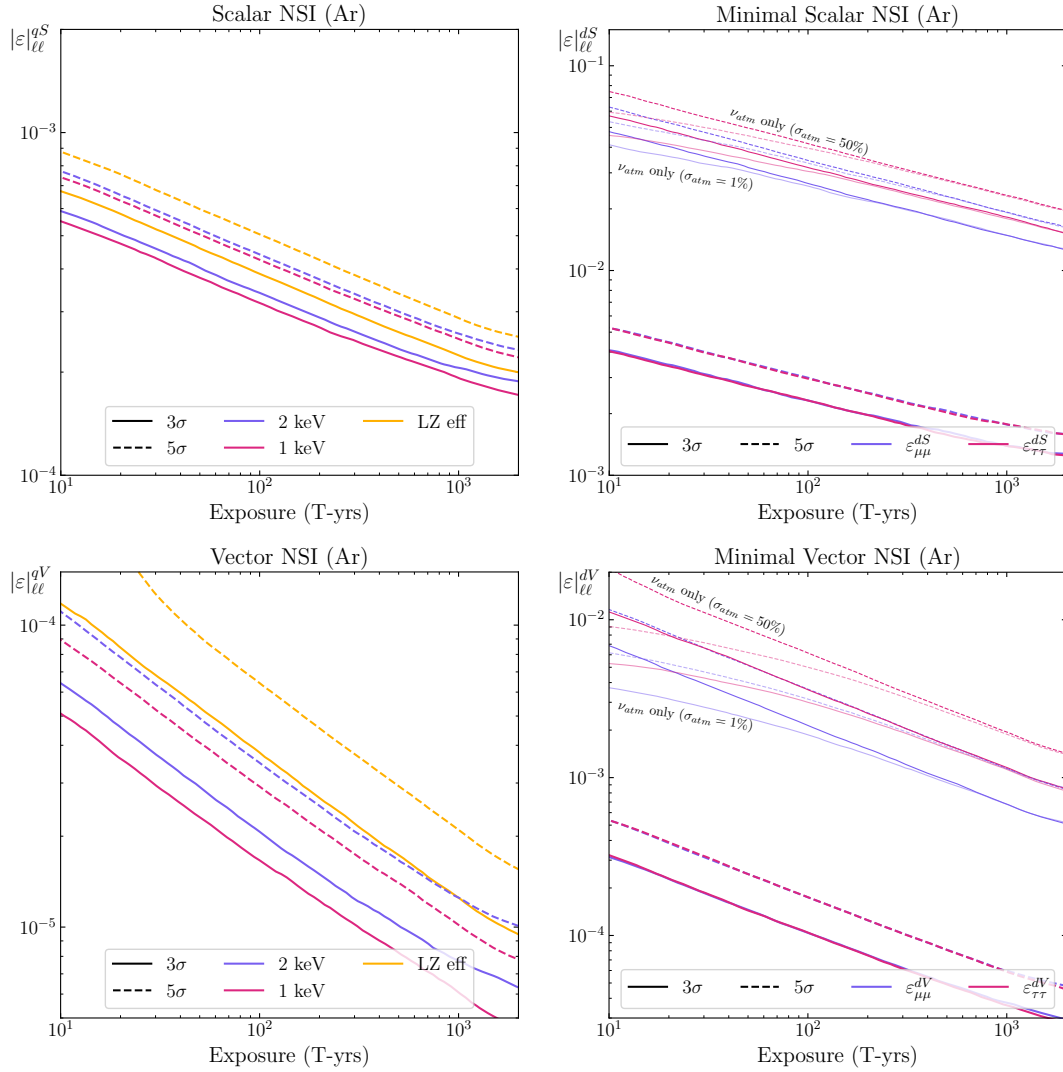


Figure 7: Left: 3σ (solid) and 5σ (dashed) discovery reach of an argon detector for a scalar (top) or vector (bottom) NSI with universal couplings as a function of detector exposure, for a 1 keV (magenta) and 2 keV (purple) detector threshold as defined in Sec. 2.1. As expected, a lower threshold improves the discovery reach. Due to its larger target mass, kinematics disfavors lead detectors despite the increased scattering rate. This is also responsible for the more dramatic improvement with detector threshold in lead. **Right:** discovery reach of an argon detector to scalar (top) or vector (bottom) NSIs coupling only the d quark to either ν_μ or ν_τ , assuming a 2 keV threshold. Thin lines indicate the sensitivity based only on atmospheric neutrinos. Fainter lines show the improvement to be gained from more precise measurement of the atmospheric neutrino flux.

V.T. was supported in part by the World Premier International Research Center Initiative (WPI), MEXT, Japan and also by JSPS KAKENHI grant No. 23K13109.

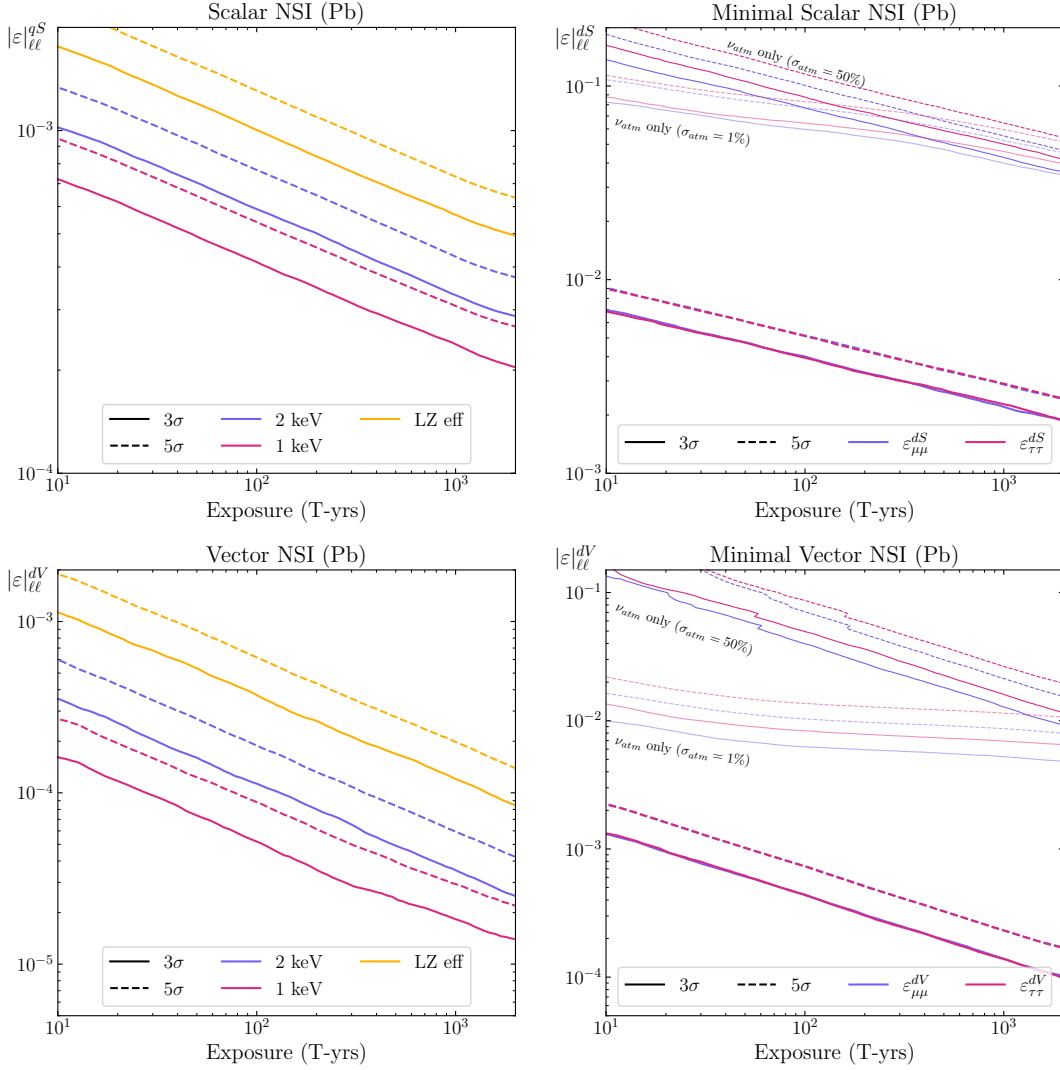


Figure 8: Same as Fig. 7, but for a lead detector. Note that due to its heavier nucleus, lead loses more sensitivity than argon or xenon at higher thresholds, and gains more from higher energy neutrinos such as the atmospheric flux.

A Model extension and neutrino mass

Following Ref. [83], we discuss a simple model extension of the S_1 LQ with a second scalar LQ, $\tilde{R}_2 = (3, 2, 1/6)$, that is an $SU(2)$ doublet ($R^{+2/3}, R^{-1/3}$), which can readily result in Majorana neutrino mass generation at one-loop level. The considered LQs can arise in a variety of theoretical frameworks, such as models of R -parity violating supersymmetry [74, 75]. The additional Lagrangian terms due to \tilde{R}_2 are

$$\mathcal{L}_{\tilde{R}_2} \supset (\tilde{\lambda}^{il} \bar{d}_R^i \tilde{R}_2 \varepsilon L_\ell + \mu H^\dagger \tilde{R}_2 S_1^* + h.c.) - m_{\tilde{R}_2}^2 |\tilde{R}_2|^2, \quad (\text{A.1})$$

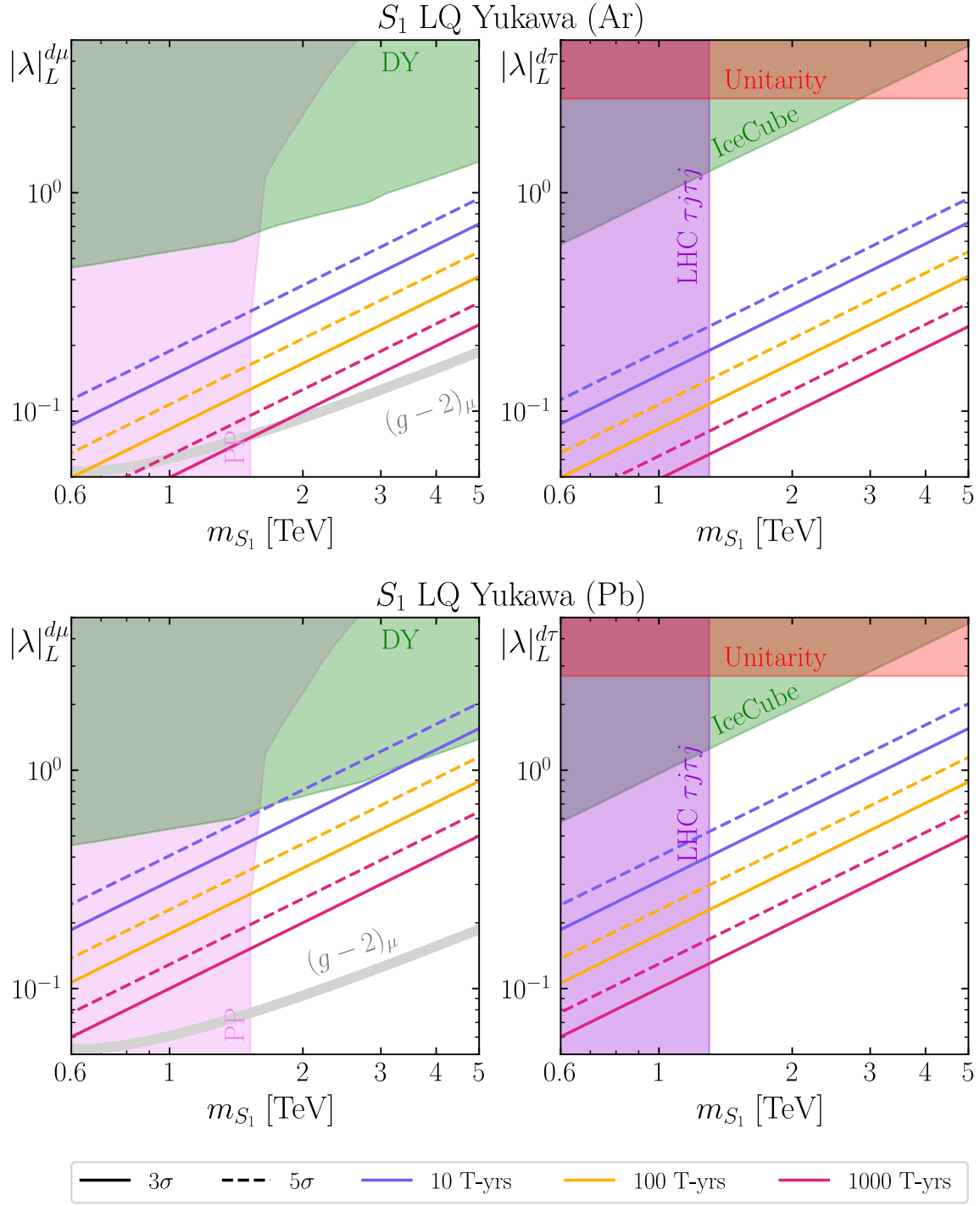


Figure 9: Same as Fig. 6, but for argon (top) and lead (bottom).

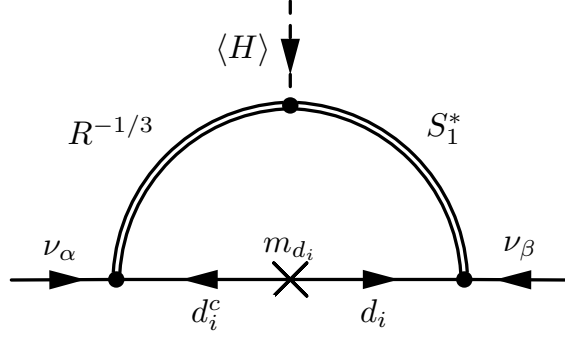


Figure 10: One-loop neutrino mass generation in the $S_1 + \tilde{R}_2$ LQ model.

where the μ -term mixes S_1 and \tilde{R}_2 LQs and $H = (1, 2, 1/2)$ is the SM Higgs doublet.

At loop-level, S_1 and \tilde{R}_2 LQs generate neutrino mass, as displayed in Fig. 10. Expanding the $SU(2)$ doublets, the necessary terms to generate neutrino NSI and masses are

$$\mathcal{L}_{S_1, \tilde{R}_2} \supset \tilde{\lambda}^{i\ell} \left(\nu_\ell \bar{d}_i R^{-1/3} - \ell \bar{d}_i R^{+2/3} \right) + \lambda_L^{i\ell} (\nu_\ell d_i - \ell \bar{u}_i^c) S_1 - \mu R^{-1/3} H^0 S_1^* + h.c. \quad (\text{A.2})$$

The mixing term implies the existence of a new LQ mass basis with eigenvalues

$$m_{1,2}^2 = \frac{1}{2} \left(m_{R^{+2/3}}^2 + m_{S_1}^2 \mp \sqrt{(m_{R^{-1/3}}^2 - m_{S_1}^2)^2 + 4\mu^2 v^2} \right) \quad (\text{A.3})$$

and a mixing angle

$$\tan(2\theta) = \frac{-\sqrt{2}\mu v}{m_{S_1}^2 - m_{R^{-1/3}}^2}, \quad (\text{A.4})$$

where v is the Higgs vev and $m_{R^{-1/3}, S_1}$ include the bare masses and the mass induced by spontaneous symmetry breaking. The neutrino mass matrix is given by

$$M_\nu = \frac{3 \sin(2\theta)}{32\pi^2} \log \left(\frac{m_1^2}{m_2^2} \right) (\tilde{\lambda} M_d \lambda_L^T + \lambda_L M_d \tilde{\lambda}^T) \quad (\text{A.5})$$

where M_d is a diagonal matrix of down-type quark masses. In the case of a LQ coupled only to down-type quarks and leptons, Eq. (A.5) simplifies to

$$(M_\nu)^{\alpha\beta} = \frac{3 \sin(2\theta)}{32\pi^2} \log \left(\frac{m_1^2}{m_2^2} \right) m_d \times (\lambda_L^{d\alpha} \tilde{\lambda}^{d\beta} + \tilde{\lambda}^{d\alpha} \lambda_L^{d\beta}), \quad (\text{A.6})$$

and similarly for LQs coupled to only strange or bottom quarks with $m_d \rightarrow m_{s,b}$. In the specific cases we study, only one element of $\lambda_L^{d\alpha}$ is non-zero implying only the generation of a single neutrino mass. However, the \tilde{R}_2 coupling $\tilde{\lambda}^{d\alpha}$ may contribute a second element to the neutrino mass matrix, or as noted in 4.1, it is possible for both $\lambda_L^{d\mu}$ and $\lambda_L^{d\tau}$ to be non-zero.

We note that with a multitude of parameters determining the neutrino mass above, there is degeneracy in LQ coupling and mass parameter space. From cosmological observations, the sum of neutrino masses given by the eigenvalues of M_ν is constrained to $\sum m_\nu < 0.13$ eV by cosmic microwave background radiation (CMB) data from Planck and the Dark Energy Survey (DES) [98].

B From leptoquarks to NSI

To map the S_1 LQ to the scalar NSI parameters, we need to find the expressions for $\varepsilon_{\ell\ell}^{dV}$ and q_S in terms of the LQ parameters. Expanding the $SU(2)_L$ doublets in eq. (4.1) and explicitly writing the hermitian conjugate, we have

$$\mathcal{L}_{S_1} \supset -m_{S_1}^2 S_1^* S_1 + \lambda_L^{1\ell} (\bar{u}^c P_L \ell - \bar{d}^c P_L \nu_\ell) S_1 + \lambda_L^{*1\ell} (\bar{u}^c P_L \ell - \bar{d}^c P_L \nu_\ell)^\dagger S_1^* \quad (\text{B.1})$$

Where we've specified $q = 1$ for the u and d quarks. Since we are considering massive scalars of $\mathcal{O}(\text{TeV})$, we can integrate out the LQ using the equations of motion

$$\begin{aligned} \frac{\partial \mathcal{L}_{S_1}}{\partial S^*} &= -m_{S_1}^2 S_1 + \lambda_L^{*1\ell} (\bar{u}^c P_L \ell - \bar{d}^c P_L \nu_\ell)^\dagger = 0 \\ \frac{\partial \mathcal{L}_{S_1}}{\partial S} &= -m_{S_1}^2 S_1^* + \lambda_L^{1\ell} (\bar{u}^c P_L \ell - \bar{d}^c P_L \nu_\ell) = 0 \end{aligned} \quad (\text{B.2})$$

and find

$$\mathcal{L}_{S_1} \supset \frac{|\lambda_L^{1\ell}|^2}{m_{S_1}^2} \left[(\bar{u}^c P_L \ell)(\bar{u}^c P_L \ell)^\dagger - (\bar{u}^c P_L \ell)(\bar{d}^c P_L \nu_\ell)^\dagger - (\bar{d}^c P_L \nu_\ell)(\bar{u}^c P_L \ell)^\dagger + (\bar{d}^c P_L \nu_\ell)(\bar{d}^c P_L \nu_\ell)^\dagger \right] \quad (\text{B.3})$$

We now focus on the last term which introduces an effective four-Fermi interaction between d quarks and neutrinos.

$$\mathcal{L}_{S_1} \supset \frac{|\lambda_L^{1\ell}|^2}{m_{S_1}^2} (\bar{d}^c P_L \nu_\ell)(\nu_\ell^\dagger P_L (\bar{d}^c)^\dagger) = \frac{|\lambda_L^{1\ell}|^2}{m_{S_1}^2} (\bar{d}^c P_L \nu_\ell)(\bar{\nu}_\ell P_R d^c) \quad (\text{B.4})$$

After a Fierz transformation [99], this becomes

$$\mathcal{L}_{S_1} \supset -\frac{|\lambda_L^{1\ell}|^2}{2m_{S_1}^2} (\bar{d}^c \gamma_\mu P_R d^c)(\bar{\nu}_\ell \gamma_\mu P_L \nu_\ell) \quad (\text{B.5})$$

Now we evaluate the charge conjugation of the quarks and find

$$\mathcal{L}_{S_1} \supset \frac{|\lambda_L^{1\ell}|^2}{2m_{S_1}^2} (\bar{d} \gamma_\mu P_L d)(\bar{\nu}_\ell \gamma_\mu P_L \nu_\ell) \quad (\text{B.6})$$

Finally, noting that we get no RH coupling and $\varepsilon_{\ell\ell}^{qV} = \varepsilon_{\ell\ell}^{qL} + \varepsilon_{\ell\ell}^{qR}$ we find that the S_1 LQ maps to Eq. (3.3) with

$$\varepsilon_{\ell\ell,S_1}^{dV} = \frac{-|\lambda_L^{d\ell}|^2}{4\sqrt{2}G_F m_{S_1}^2}. \quad (\text{B.7})$$

We note that the NSI parameter resulting from an S_1 LQ is negative.

C Neutrino oscillation effects

In Sec. 2 we briefly discussed the effects of neutrino oscillations. Here, we expand the discussion and consider neutrino oscillations with and without NSI effects in neutrino propagation through the Earth or Sun. To analyze neutrino propagation through Earth we use the NuCraft code [100], which is based on the PREM Earth reference model⁸ [101], and include modifications for vector neutrino NSI [65, 102, 103] and scalar neutrino NSI [66]. For solar neutrinos, full in-medium effects and NSI are already built into the SNUDD module [104] that we use to calculate the flavor dependence of the solar neutrinos when they reach Earth. In all cases we assume normal neutrino mass ordering.

In the case of vector NSI, the contributions to the matter potential result in the effective Hamiltonian

$$\mathcal{H}_{\text{vNSI,matter}} \simeq E_\nu + \frac{MM^\dagger}{2E_\nu} \pm (V_{\text{SI}} + V_{\text{NSI}}), \quad (\text{C.1})$$

where the neutrino mass matrix M , SM matter potential V_{SI} , and the vector NSI matter potential contributions V_{NSI} are 3×3 matrices. The matter potential becomes significant only when the neutrino energy E_ν or matter density are sizable $2E_\nu V \gtrsim \Delta m_{ij}^2$ [66]. Flavor conserving NSI in the $\mu - \tau$ sector can be parameterized by a single parameter $\varepsilon_{\tau\tau} - \varepsilon_{\mu\mu}$ where $\varepsilon_{\ell\ell} = \sum_f Y_f \varepsilon_{\ell\ell}^{fV}$ is the sum of couplings to each fermion weighted by the fermion number density Y_f (relative to Y_e). In this parameterization, current experimental limits are $|\varepsilon_{\ell\ell}| \lesssim 0.04$ [90] in $\mu - \tau$ sector. Constraints on flavor violating NSI from oscillations are much stronger since they have a greater effect on oscillation probabilities, but we do not consider these NSI in this work.

In Fig. 11 we display the oscillation probabilities for a characteristic vector NSI values we consider $|\varepsilon_{\tau\tau}^{qV}| \sim 10^{-2}$ along with the SM medium effects inside the Earth. For the SM effects, we find reasonable agreement with [105]. Note that effects of a coupling to up or down quarks are similar, since the NSI potential scales with Y_u and Y_d respectively. From Fig. 11 we observe that at particular propagation directions with respect to zenith⁹ and neutrino energies vector NSI $\varepsilon \sim 0.01$ can modify flavor oscillation by $\mathcal{O}(10\%)$. Here we do not consider detectors with directional sensitivity. Hence, integrating the atmospheric flux contributions over the field-of-view and including recoil kinematics and detector resolution further reduces the significance

⁸NuCraft was built for IceCube and thus considers a detector 2 km deep near the south pole. Slight deviations are noted with results for different geomagnetic locations including Kamioka in Japan and Sudbury in Canada

⁹Straight down propagation is at 180° .

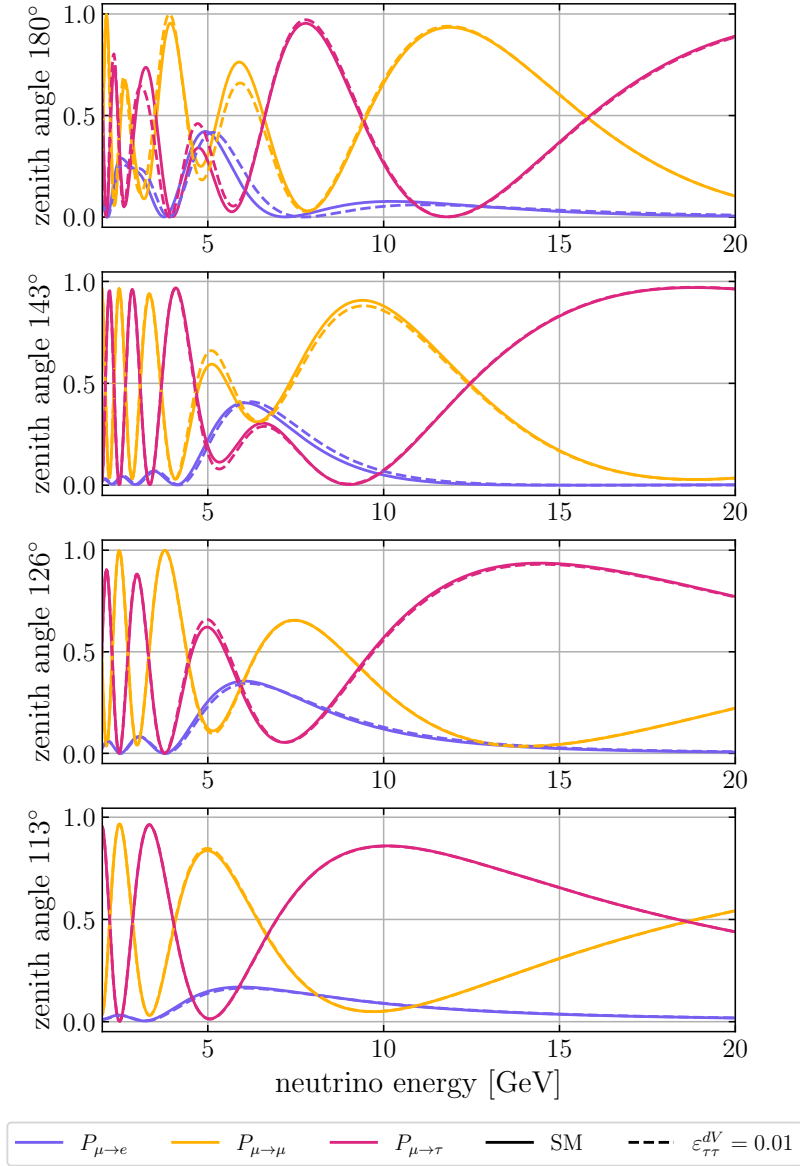


Figure 11: Oscillation conversion probabilities of atmospheric neutrinos, calculated using the NuCraft code, with (dashed line) and without (solid line) vector NSI effects for distinct directions with respect to zenith.

of the vector NSI on the signal in dark matter experiments. Further detailed study and consideration of detectors with directional sensitivity could leverage these effects to improve sensitivities to vector NSI, analysis of which we leave for future work.

The vector NSI effects are suppressed at lower neutrino energies and thus the NSI parameters we consider have negligible effect on solar neutrinos despite the increase in medium density. In Fig. 12 we display oscillation probabilities for solar neutrinos as calculated using

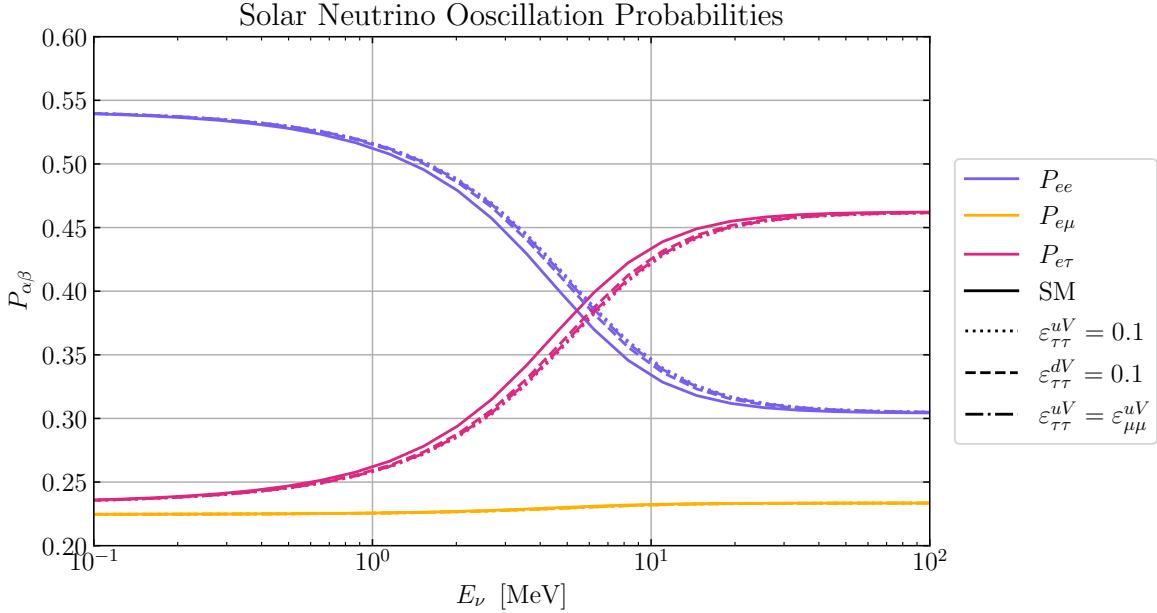


Figure 12: Oscillation conversion probabilities of solar neutrinos, as calculated with the SNUDD module, for SM (solid line) and including vector NSI coupling of tau neutrinos to up quarks (dotted line), down quarks (dashed line), or both (dot-dashed line).

SNUDD package considering NSI of $\varepsilon = 0.1$, which is significantly larger than the parameters we consider in this work. Solar neutrino oscillations in vacuum are also considered, though are subdominant to the medium effects. We assume a constant Earth-Sun distance of 1.5×10^8 km. Qualitatively, we have found agreement of our considerations with discussion in Ref. [106].

In contrast to vector NSI, scalar NSI induce an effective correction to the neutrino mass matrix, which scales with the matter density and is suppressed by the neutrino energy. This leads to a neutrino oscillation probability that is sensitive to the matter density variations along the propagation baseline [66]. In the flavor basis, $M_{eff} = M + M_{\text{NSI}}$ where M is the standard neutrino mass matrix and $M_{\text{NSI}} = \sum_q n_q G_F \varepsilon_{\ell\ell}^{qS}$ where $\varepsilon_{\ell\ell}^{qS}$ is the scalar NSI parameter in Eq. (3.1) and n_q is the quark number density. We focus on flavor conserving NSIs, so M_{NSI} is diagonal in the flavor basis¹⁰. Transforming to the mass basis and rotating the phasing matrix into the NSI term, M_{eff} is given in Eq. (C.2) where $D_\nu = \text{diag}(m_1, m_2, m_3)$ ¹¹ is the diagonal neutrino mass matrix, \mathcal{U} is the PMNS matrix, and P is the diagonal rephasing matrix

$$M_{eff} = \mathcal{U} D_\nu \mathcal{U}^\dagger + P^\dagger M_{\text{NSI}} P. \quad (\text{C.2})$$

Following the notation of Ref. [66], we take $\sqrt{|\Delta m_{31}^2|}$ as a characteristic mass scale and

¹⁰In general, $\varepsilon_{\alpha\beta}^{qS}$ are also possible.

¹¹ $\text{diag}(x, y, z)$ is defined as the 3×3 diagonal matrix with elements x, y, z on the diagonal.

parameterize the NSI mass contribution as

$$P^\dagger M_{\text{NSI}} P = \delta M = \sqrt{|\Delta m_{31}^2|} (\eta)_{i,j} \quad (\text{C.3})$$

where $(\eta)_{i,j}$ are matrix elements in the mass basis. For neutrinos propagating in matter with scalar NSI contributions, the effective Hamiltonian is

$$\mathcal{H}_{\text{sNSI,matter}} = E_\nu + \frac{M_{\text{eff}} M_{\text{eff}}^\dagger}{2E_\nu} + V_{\text{SI}} , \quad (\text{C.4})$$

where V_{SI} is the SM matter potential from charged-current interactions. For antineutrinos, V_{SI} changes sign. At the energies and couplings we consider in the analysis, SM vector interactions contribute significantly more strongly to neutrino oscillations than scalar NSI, such that the latter do not have appreciable effects in dark matter experiments.

References

- [1] LZ collaboration, J. Aalbers et al., *First Dark Matter Search Results from the LUX-ZEPLIN (LZ) Experiment*, [2207.03764](#).
- [2] XENON collaboration, E. Aprile et al., *First Dark Matter Search with Nuclear Recoils from the XENONnT Experiment*, [2303.14729](#).
- [3] DEAP collaboration, R. Ajaj et al., *Search for dark matter with a 231-day exposure of liquid argon using DEAP-3600 at SNOLAB*, *Phys. Rev. D* **100** (2019) 022004 [[1902.04048](#)].
- [4] DARKSIDE-50 collaboration, P. Agnes et al., *Search for low-mass dark matter WIMPs with 12 ton-day exposure of DarkSide-50*, *Phys. Rev. D* **107** (2023) 063001 [[2207.11966](#)].
- [5] D. Z. Freedman, *Coherent Neutrino Nucleus Scattering as a Probe of the Weak Neutral Current*, *Phys. Rev. D* **9** (1974) 1389.
- [6] A. Drukier and L. Stodolsky, *Principles and Applications of a Neutral Current Detector for Neutrino Physics and Astronomy*, *Phys. Rev. D* **30** (1984) 2295.
- [7] COHERENT collaboration, D. Akimov et al., *Observation of Coherent Elastic Neutrino-Nucleus Scattering*, *Science* **357** (2017) 1123 [[1708.01294](#)].
- [8] CONUS collaboration, H. Bonet et al., *Novel constraints on neutrino physics beyond the standard model from the CONUS experiment*, *JHEP* **05** (2022) 085 [[2110.02174](#)].
- [9] CONNIE collaboration, A. Aguilar-Arevalo et al., *Results of the Engineering Run of the Coherent Neutrino Nucleus Interaction Experiment (CONNIE)*, *JINST* **11** (2016) P07024 [[1604.01343](#)].
- [10] NUCLEUS collaboration, G. Angloher et al., *Exploring CE ν NS with NUCLEUS at the Chooz nuclear power plant*, *Eur. Phys. J. C* **79** (2019) 1018 [[1905.10258](#)].
- [11] J. Billard et al., *Coherent Neutrino Scattering with Low Temperature Bolometers at Chooz Reactor Complex*, *J. Phys. G* **44** (2017) 105101 [[1612.09035](#)].
- [12] J. Billard, E. Figueroa-Feliciano and L. Strigari, *Implication of neutrino backgrounds on the reach of next generation dark matter direct detection experiments*, *Phys. Rev. D* **89** (2014) 023524.
- [13] R. Essig, M. Sholapurkar and T.-T. Yu, *Solar Neutrinos as a Signal and Background in Direct-Detection Experiments Searching for Sub-GeV Dark Matter With Electron Recoils*, *Phys. Rev. D* **97** (2018) 095029 [[1801.10159](#)].
- [14] G. B. Gelmini, V. Takhistov and S. J. Witte, *Casting a Wide Signal Net with Future Direct Dark Matter Detection Experiments*, *JCAP* **07** (2018) 009 [[1804.01638](#)].
- [15] SUPER-KAMIOKANDE collaboration, Y. Fukuda et al., *Evidence for oscillation of atmospheric neutrinos*, *Phys. Rev. Lett.* **81** (1998) 1562 [[hep-ex/9807003](#)].
- [16] PARTICLE DATA GROUP collaboration, R. L. Workman et al., *Review of Particle Physics*, *PTEP* **2022** (2022) 083C01.
- [17] *Neutrino Non-Standard Interactions: A Status Report*, vol. 2, 2019. 10.21468/SciPostPhysProc.2.001.

- [18] Y. Farzan and J. Heeck, *Neutrinophilic nonstandard interactions*, *Phys. Rev. D* **94** (2016) 053010 [[1607.07616](#)].
- [19] J. Barranco, O. G. Miranda and T. I. Rashba, *Probing new physics with coherent neutrino scattering off nuclei*, *JHEP* **12** (2005) 021 [[hep-ph/0508299](#)].
- [20] K. Scholberg, *Prospects for measuring coherent neutrino-nucleus elastic scattering at a stopped-pion neutrino source*, *Phys. Rev. D* **73** (2006) 033005 [[hep-ex/0511042](#)].
- [21] O. G. Miranda, D. K. Papoulias, G. Sanchez Garcia, O. Sanders, M. Tórtola and J. W. F. Valle, *Implications of the first detection of coherent elastic neutrino-nucleus scattering (CE ν NS) with Liquid Argon*, *JHEP* **05** (2020) 130 [[2003.12050](#)].
- [22] J. Liao and D. Marfatia, *COHERENT constraints on nonstandard neutrino interactions*, *Phys. Lett. B* **775** (2017) 54 [[1708.04255](#)].
- [23] C. Giunti, *General COHERENT constraints on neutrino nonstandard interactions*, *Phys. Rev. D* **101** (2020) 035039 [[1909.00466](#)].
- [24] A. N. Khan, D. W. McKay and W. Rodejohann, *CP-violating and charged current neutrino nonstandard interactions in CE ν NS*, *Phys. Rev. D* **104** (2021) 015019 [[2104.00425](#)].
- [25] P. B. Denton and J. Gehrlein, *A Statistical Analysis of the COHERENT Data and Applications to New Physics*, *JHEP* **04** (2021) 266 [[2008.06062](#)].
- [26] Y. Farzan, M. Lindner, W. Rodejohann and X.-J. Xu, *Probing neutrino coupling to a light scalar with coherent neutrino scattering*, *JHEP* **05** (2018) 066 [[1802.05171](#)].
- [27] G. Arcadi, M. Lindner, J. Martins and F. S. Queiroz, *New physics probes: Atomic parity violation, polarized electron scattering and neutrino-nucleus coherent scattering*, *Nucl. Phys. B* **959** (2020) 115158 [[1906.04755](#)].
- [28] J. Billard, J. Johnston and B. J. Kavanagh, *Prospects for exploring New Physics in Coherent Elastic Neutrino-Nucleus Scattering*, *JCAP* **11** (2018) 016 [[1805.01798](#)].
- [29] E. Bertuzzo, G. Grilli di Cortona and L. M. D. Ramos, *Probing light vector mediators with coherent scattering at future facilities*, *JHEP* **06** (2022) 075 [[2112.04020](#)].
- [30] L. M. G. de la Vega, L. J. Flores, N. Nath and E. Peinado, *Complementarity between dark matter direct searches and CE ν NS experiments in $U(1)$ ' models*, *JHEP* **09** (2021) 146 [[2107.04037](#)].
- [31] H. Banerjee, B. Dutta and S. Roy, *Probing $L\mu$ - $L\tau$ models with CE ν NS: A new look at the combined COHERENT CsI and Ar data*, *Phys. Rev. D* **104** (2021) 015015 [[2103.10196](#)].
- [32] M. Cadeddu, N. Cargioli, F. Dordei, C. Giunti, Y. F. Li, E. Picciau et al., *Constraints on light vector mediators through coherent elastic neutrino nucleus scattering data from COHERENT*, *JHEP* **01** (2021) 116 [[2008.05022](#)].
- [33] L. J. Flores, N. Nath and E. Peinado, *Non-standard neutrino interactions in $U(1)$ ' model after COHERENT data*, *JHEP* **06** (2020) 045 [[2002.12342](#)].
- [34] P. B. Denton, Y. Farzan and I. M. Shoemaker, *Testing large non-standard neutrino interactions with arbitrary mediator mass after COHERENT data*, *JHEP* **07** (2018) 037 [[1804.03660](#)].

- [35] R. Harnik, J. Kopp and P. A. N. Machado, *Exploring ν Signals in Dark Matter Detectors*, *JCAP* **07** (2012) 026 [[1202.6073](#)].
- [36] D. G. Cerdeño, M. Fairbairn, T. Jubb, P. A. N. Machado, A. C. Vincent and C. Boehm, *Physics from solar neutrinos in dark matter direct detection experiments*, *JHEP* **05** (2016) 118 [[1604.01025](#)].
- [37] C. Boehm, D. G. Cerdeno, M. Fairbairn, P. A. N. Machado and A. C. Vincent, *Light new physics in XENON1T*, *Phys. Rev. D* **102** (2020) 115013 [[2006.11250](#)].
- [38] E. Bertuzzo, F. F. Deppisch, S. Kulkarni, Y. F. Perez Gonzalez and R. Zukanovich Funchal, *Dark Matter and Exotic Neutrino Interactions in Direct Detection Searches*, *JHEP* **04** (2017) 073 [[1701.07443](#)].
- [39] J. L. Newstead, R. F. Lang and L. E. Strigari, *Atmospheric neutrinos in next-generation xenon and argon dark matter experiments*, *Phys. Rev. D* **104** (2021) 115022 [[2002.08566](#)].
- [40] A. Angelescu, D. Bećirević, D. A. Faroughy and O. Sumensari, *Closing the window on single leptoquark solutions to the B-physics anomalies*, *Journal of High Energy Physics* **2018** (2018) 183.
- [41] H. M. Lee, *Leptoquark option for B-meson anomalies and leptonic signatures*, *Phys. Rev. D* **104** (2021) 015007 [[2104.02982](#)].
- [42] P. Fileviez Perez, C. Murgui and A. D. Plascencia, *Leptoquarks and matter unification: Flavor anomalies and the muon $g-2$* , *Phys. Rev. D* **104** (2021) 035041 [[2104.11229](#)].
- [43] I. Doršner, S. Fajfer and N. Košnik, *Leptoquark mechanism of neutrino masses within the grand unification framework*, *Eur. Phys. J. C* **77** (2017) 417 [[1701.08322](#)].
- [44] D. Zhang, *Radiative neutrino masses, lepton flavor mixing and muon $g-2$ in a leptoquark model*, *Journal of High Energy Physics* **2021** (2021) 69.
- [45] D. Aristizabal Sierra, M. Hirsch and S. G. Kovalenko, *Leptoquarks: Neutrino masses and related accelerator signals*, *Phys. Rev. D* **77** (2008) 055011.
- [46] Y.-F. Li and S. yu Xia, *Constraining light mediators via detection of coherent elastic solar neutrino nucleus scattering*, *Nuclear Physics B* **977** (2022) 115737.
- [47] A. Majumdar, D. K. Papoulias and R. Srivastava, *Dark matter detectors as a novel probe for light new physics*, *Phys. Rev. D* **106** (2022) 013001.
- [48] P. deNiverville, M. Pospelov and A. Ritz, *Light new physics in coherent neutrino-nucleus scattering experiments*, *Phys. Rev. D* **92** (2015) 095005 [[1505.07805](#)].
- [49] T. Schwemberger and T.-T. Yu, *Detecting beyond the standard model interactions of solar neutrinos in low-threshold dark matter detectors*, *Phys. Rev. D* **106** (2022) 015002 [[2202.01254](#)].
- [50] J. A. Formaggio and G. P. Zeller, *From eV to EeV: Neutrino Cross Sections Across Energy Scales*, *Rev. Mod. Phys.* **84** (2012) 1307 [[1305.7513](#)].
- [51] J. Lewin and P. Smith, *Review of mathematics, numerical factors, and corrections for dark matter experiments based on elastic nuclear recoil*, *Astroparticle Physics* **6** (1996) 87.
- [52] R. H. Helm, *Inelastic and elastic scattering of 187-mev electrons from selected even-even nuclei*, *Phys. Rev.* **104** (1956) 1466.

- [53] N. Vinyoles, A. M. Serenelli, F. L. Villante, S. Basu, J. Bergström, M. C. Gonzalez-Garcia et al., *A new Generation of Standard Solar Models*, *Astrophys. J.* **835** (2017) 202 [[1611.09867](#)].
- [54] G. Battistoni, A. Ferrari, T. Montaruli and P. R. Sala, *The atmospheric neutrino flux below 100-MeV: The FLUKA results*, *Astropart. Phys.* **23** (2005) 526.
- [55] S. Horiuchi, J. F. Beacom and E. Dwek, *The Diffuse Supernova Neutrino Background is detectable in Super-Kamiokande*, *Phys. Rev. D* **79** (2009) 083013 [[0812.3157](#)].
- [56] Y. Huang, V. Chubakov, F. Mantovani, R. L. Rudnick and W. F. McDonough, *A reference Earth model for the heat producing elements and associated geoneutrino flux*, *arXiv e-prints* (2013) [arXiv:1301.0365](#) [[1301.0365](#)].
- [57] W. C. Haxton, R. G. Hamish Robertson and A. M. Serenelli, *Solar Neutrinos: Status and Prospects*, *Ann. Rev. Astron. Astrophys.* **51** (2013) 21 [[1208.5723](#)].
- [58] J. N. Bahcall, A. M. Serenelli and S. Basu, *New solar opacities, abundances, helioseismology, and neutrino fluxes*, *Astrophys. J. Lett.* **621** (2005) L85 [[astro-ph/0412440](#)].
- [59] BOREXINO collaboration, S. Appel et al., *Improved Measurement of Solar Neutrinos from the Carbon-Nitrogen-Oxygen Cycle by Borexino and Its Implications for the Standard Solar Model*, *Phys. Rev. Lett.* **129** (2022) 252701 [[2205.15975](#)].
- [60] J. F. Beacom, *The Diffuse Supernova Neutrino Background*, *Ann. Rev. Nucl. Part. Sci.* **60** (2010) 439 [[1004.3311](#)].
- [61] SUPER-KAMIOKANDE collaboration, K. Abe et al., *Diffuse supernova neutrino background search at Super-Kamiokande*, *Phys. Rev. D* **104** (2021) 122002 [[2109.11174](#)].
- [62] T. K. Gaisser and M. Honda, *Flux of atmospheric neutrinos*, *Ann. Rev. Nucl. Part. Sci.* **52** (2002) 153 [[hep-ph/0203272](#)].
- [63] Y. Zhuang, L. E. Strigari and R. F. Lang, *Time variation of the atmospheric neutrino flux at dark matter detectors*, *Phys. Rev. D* **105** (2022) 043001.
- [64] L. Wolfenstein, *Neutrino Oscillations in Matter*, *Phys. Rev. D* **17** (1978) 2369.
- [65] A. Friedland, C. Lunardini and C. Pena-Garay, *Solar neutrinos as probes of neutrino matter interactions*, *Phys. Lett. B* **594** (2004) 347 [[hep-ph/0402266](#)].
- [66] S.-F. Ge and S. J. Parke, *Scalar Nonstandard Interactions in Neutrino Oscillation*, *Phys. Rev. Lett.* **122** (2019) 211801 [[1812.08376](#)].
- [67] P. S. B. Dev, K. S. Babu, P. B. Denton, P. A. N. Machado, C. A. Argüelles, J. L. Barrow et al., *Neutrino non-standard interactions: A status report*, *SciPost Phys. Proc.* (2019) 001.
- [68] M. Lindner, W. Rodejohann and X.-J. Xu, *Coherent neutrino-nucleus scattering and new neutrino interactions*, *Journal of High Energy Physics* **2017** (2017) 97.
- [69] K. S. Babu, G. Chauhan and P. S. B. Dev, *Neutrino nonstandard interactions via light scalars in the earth, sun, supernovae, and the early universe*, *Phys. Rev. D* **101** (2020) 095029.
- [70] H. Georgi and S. L. Glashow, *Unity of All Elementary Particle Forces*, *Phys. Rev. Lett.* **32** (1974) 438.

- [71] H. Fritzsch and P. Minkowski, *Unified Interactions of Leptons and Hadrons*, *Annals Phys.* **93** (1975) 193.
- [72] H. Georgi, *The State of the Art—Gauge Theories*, *AIP Conf. Proc.* **23** (1975) 575.
- [73] J. C. Pati and A. Salam, *Lepton Number as the Fourth Color*, *Phys. Rev. D* **10** (1974) 275.
- [74] L. J. Hall and M. Suzuki, *Explicit R-Parity Breaking in Supersymmetric Models*, *Nucl. Phys. B* **231** (1984) 419.
- [75] R. Barbier et al., *R-parity violating supersymmetry*, *Phys. Rept.* **420** (2005) 1 [[hep-ph/0406039](#)].
- [76] HFLAV collaboration, Y. S. Amhis et al., *Averages of b -hadron, c -hadron, and τ -lepton properties as of 2018*, *Eur. Phys. J. C* **81** (2021) 226 [[1909.12524](#)].
- [77] LHCb collaboration, R. Aaij et al., *Test of lepton universality in beauty-quark decays*, *Nature Phys.* **18** (2022) 277 [[2103.11769](#)].
- [78] I. Doršner, S. Fajfer and O. Sumensari, *Muon $g-2$ and scalar leptoquark mixing*, *Journal of High Energy Physics* **2020** (2020) 89.
- [79] V. Gherardi, D. Marzocca and E. Venturini, *Low-energy phenomenology of scalar leptoquarks at one-loop accuracy*, *Journal of High Energy Physics* **2021** (2021) 138.
- [80] M. Schmaltz and Y.-M. Zhong, *The leptoquark Hunter’s guide: large coupling*, *JHEP* **01** (2019) 132 [[1810.10017](#)].
- [81] I. Doršner, S. Fajfer, A. Greljo, J. Kamenik and N. Košnik, *Physics of leptoquarks in precision experiments and at particle colliders*, *Physics Reports* **641** (2016) 1.
- [82] D. Aristizabal Sierra, M. Hirsch and S. G. Kovalenko, *Leptoquarks: Neutrino masses and accelerator phenomenology*, *Phys. Rev. D* **77** (2008) 055011 [[0710.5699](#)].
- [83] K. S. Babu, P. S. B. Dev, S. Jana and A. Thapa, *Non-Standard Interactions in Radiative Neutrino Mass Models*, *JHEP* **03** (2020) 006 [[1907.09498](#)].
- [84] K. S. Babu, P. S. B. Dev, S. Jana and A. Thapa, *Unified framework for b -anomalies, muon $g - 2$ and neutrino masses*, *JHEP* **03** (2021) 179 [[2009.01771](#)].
- [85] B. Diaz, M. Schmaltz and Y.-M. Zhong, *The leptoquark Hunter’s guide: Pair production*, *JHEP* **10** (2017) 097 [[1706.05033](#)].
- [86] B. M. Roberts, V. A. Dzuba and V. V. Flambaum, *Parity and Time-Reversal Violation in Atomic Systems*, *Ann. Rev. Nucl. Part. Sci.* **65** (2015) 63 [[1412.6644](#)].
- [87] QWEAK collaboration, D. Androić et al., *Precision measurement of the weak charge of the proton*, *Nature* **557** (2018) 207 [[1905.08283](#)].
- [88] D. Zhang, *Radiative neutrino masses, lepton flavor mixing and muon $g - 2$ in a leptoquark model*, *JHEP* **07** (2021) 069 [[2105.08670](#)].
- [89] M. Bauer and M. Neubert, *Minimal leptoquark explanation for the $R_{D^{(*)}}$, R_K , and $(g - 2)_\mu$ anomalies*, *Phys. Rev. Lett.* **116** (2016) 141802.
- [90] ICECUBE COLLABORATION collaboration, R. Abbasi et al., *All-flavor constraints on nonstandard neutrino interactions and generalized matter potential with three years of icecube deepcore data*, *Phys. Rev. D* **104** (2021) 072006.

- [91] THE SUPER-KAMIOKANDE COLLABORATION collaboration, G. Mitsuka, K. Abe, Y. Hayato, T. Iida, M. Ikeda, J. Kameda et al., *Study of nonstandard neutrino interactions with atmospheric neutrino data in super-kamiokande i and ii*, *Phys. Rev. D* **84** (2011) 113008.
- [92] LUX-ZEPLIN COLLABORATION collaboration, J. Aalbers et. al., *First dark matter search results from the lux-zeplin (lz) experiment*, 2022. 10.48550/ARXIV.2207.03764.
- [93] CMS COLLABORATION collaboration, *Search for pair production of second-generation leptoquarks at $\sqrt{s} = 13$ TeV*, *Phys. Rev. D* **99** (2019) 032014.
- [94] CMS COLLABORATION collaboration, *Search for high-mass resonances in dilepton final states in proton-proton collisions at $\sqrt{s} = 13$ TeV*, *Journal of High Energy Physics* **2018** (2018) 120.
- [95] A. Collaboration, *Search for excited τ -leptons and leptoquarks in the final state with τ -leptons and jets in pp collisions at $\sqrt{s} = 13$ tev with the atlas detector*, 2023.
- [96] K. S. Babu, P. S. B. Dev and S. Jana, *Probing neutrino mass models through resonances at neutrino telescopes*, *Int. J. Mod. Phys. A* **37** (2022) 2230003 [2202.06975].
- [97] L. Allwicher, P. Arnan, D. Barducci and M. Nardecchia, *Perturbative unitarity constraints on generic Yukawa interactions*, *Journal of High Energy Physics* **2021** (2021) 129.
- [98] DES AND SPT COLLABORATIONS collaboration, T. M. C. Abbott, M. Aguena, A. Alarcon, O. Alves, A. Amon, F. Andrade-Oliveira et al., *Joint analysis of dark energy survey year 3 data and cmb lensing from spt and planck. iii. combined cosmological constraints*, *Phys. Rev. D* **107** (2023) 023531.
- [99] I. Bischer, W. Rodejohann and X.-J. Xu, *Loop-induced neutrino non-standard interactions*, *Journal of High Energy Physics* **2018** (2018) 96.
- [100] M. Wallraff and C. Wiebusch, *Calculation of oscillation probabilities of atmospheric neutrinos using nuCraft*, *Comput. Phys. Commun.* **197** (2015) 185 [1409.1387].
- [101] A. M. Dziewonski and D. L. Anderson, *Preliminary reference earth model*, *Phys. Earth Planet. Interiors* **25** (1981) 297.
- [102] M. C. Gonzalez-Garcia and M. Maltoni, *Determination of matter potential from global analysis of neutrino oscillation data*, *JHEP* **09** (2013) 152 [1307.3092].
- [103] P. Coloma, P. B. Denton, M. C. Gonzalez-Garcia, M. Maltoni and T. Schwetz, *Curtailling the Dark Side in Non-Standard Neutrino Interactions*, *JHEP* **04** (2017) 116 [1701.04828].
- [104] D. W. P. Amaral, D. Cerdeno, A. Cheek and P. Foldenauer, *A direct detection view of the neutrino NSI landscape*, *JHEP* **07** (2023) 071 [2302.12846].
- [105] SUPER-KAMIOKANDE collaboration, K. Abe et al., *Atmospheric neutrino oscillation analysis with external constraints in Super-Kamiokande I-IV*, *Phys. Rev. D* **97** (2018) 072001 [1710.09126].
- [106] M. Maltoni and A. Y. Smirnov, *Solar neutrinos and neutrino physics*, *Eur. Phys. J. A* **52** (2016) 87 [1507.05287].